Roles of the Equatorial Tyrosyl Iron Ligand of Protocatechuate 3,4-Dioxygenase in Catalysis † , ‡

ARTICLE *in* BIOCHEMISTRY · SEPTEMBER 2005

Impact Factor: 3.02 · DOI: 10.1021/bi050902i · Source: PubMed

6 AUTHORS, INCLUDING:

Michael P Valley
Promega
29 PUBLICATIONS **542** CITATIONS
SEE PROFILE

Matthew Vetting
Albert Einstein College of Medicine
60 PUBLICATIONS **1,913** CITATIONS
SEE PROFILE

BIOCHEMISTRY
including biophysical chemistry & molecular biology

Article

Roles of the Equatorial Tyrosyl Iron Ligand of Protocatechuate 3,4-Dioxygenase in Catalysis

Michael P. Valley, C. Kent Brown, David L. Burk, Matthew W. Vetting, Douglas H. Ohlendorf, and John D. Lipscomb

Biochemistry, **2005**, 44 (33), 11024-11039 • DOI: 10.1021/bi050902i

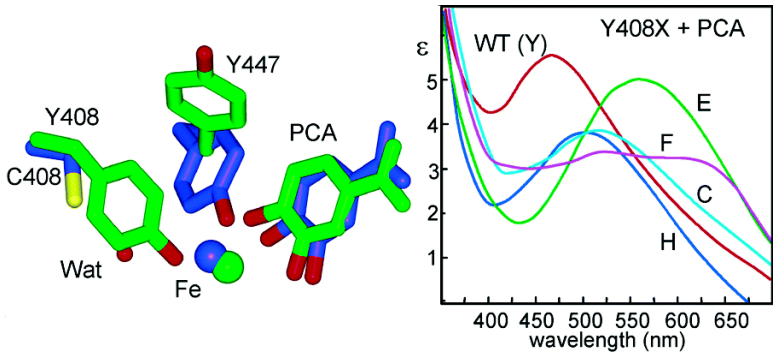

More About This Article

Additional resources and features associated with this article are available within the HTML version:

- Supporting Information
- Links to the 4 articles that cite this article, as of the time of this article download
- Access to high resolution figures
- Links to articles and content related to this article
- Copyright permission to reproduce figures and/or text from this article

View the Full Text HTML

Roles of the Equatorial Tyrosyl Iron Ligand of Protocatechuate 3,4-Dioxygenase in Catalysis[†,‡]

Michael P. Valley,[§] C. Kent Brown,[∥] David L. Burk,[⊥] Matthew W. Vetting,[#] Douglas H. Ohlendorf,* and John D. Lipscomb*

Department of Biochemistry, Molecular Biology, and Biophysics and Center for Metals in Biocatalysis, University of Minnesota, Minneapolis, Minnesota 55455

Received May 14, 2005; Revised Manuscript Received June 20, 2005

ABSTRACT: The active site Fe(III) of protocatechuate 3,4-dioxygenase (3,4-PCD) from *Pseudomonas putida* is ligated axially by Tyr447 and His462 and equatorially by Tyr408, His460, and OH^-. Tyr447 and OH^- are displaced as protocatechuate (3,4-dihydroxybenzoate, PCA) chelates the iron and appear to serve as in situ bases to promote this process. The role(s) of Tyr408 is (are) explored here using mutant enzymes that exhibit less than 0.1% wild-type activity. The X-ray crystal structures of the mutants and their PCA complexes show that the new shorter residues in the 408 position cannot ligate the iron and instead interact with the iron through solvents. Moreover, PCA binds as a monodentate rather than a bidentate ligand, and Tyr447 fails to dissociate. Although the new residues at position 408 do not directly bind to the iron, large changes in the spectroscopic and catalytic properties are noted among the mutant enzymes. Resonance Raman features show that the Fe−O bond of the monodentate 4-hydroxybenzoate (4HB) inhibitor complex is significantly stronger in the mutants than in wild-type 3,4-PCD. Transient kinetic studies show that PCA and 4HB bind to 3,4-PCD in a fast, reversible step followed by a step in which coordination to the metal occurs; the latter process is at least 50-fold slower in the mutant enzymes. It is proposed that, in wild-type 3,4-PCD, the Lewis base strength of Tyr408 lowers the Lewis acidity of the iron to foster the rapid exchange of anionic ligands during the catalytic cycle. Accordingly, the increase in Lewis acidity of the iron caused by substitution of this residue by solvent tends to make the iron substitution inert. Tyr447 cannot be released to allow formation of the usual dianionic PCA chelate complex with the active site iron, and the rate of electrophilic attack by O_2 becomes rate limiting overall. The structures of the PCA complexes of these mutant enzymes show that hydrogen-bonding interactions between the new solvent ligand and the new second-sphere residue in position 408 allow this residue to significantly influence the spectroscopic and kinetic properties of the enzymes.

Protocatechuate 3,4-dioxygenase (3,4-PCD)[1] (E.C. 1.13.11.3) catalyzes the ring cleavage of protocatechuate (PCA, 3,4-dihydroxybenzoate) with the incorporation of both atoms of molecular oxygen to form β-carboxy-*cis*,*cis*-muconate (*1*, *2*).

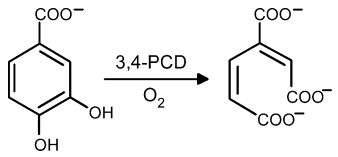

This is a critical step in the bacterial assimilation of aromatic carbon as part of the β-ketoadipate catabolic pathway (*3*). The enzyme from *Pseudomonas putida* (reclassified from *Pseudomonas aeruginosa*) is a 587 kDa dodecamer composed of $\alpha\beta$ heterodimers, each binding a single ferric ion. The crystal structure of the enzyme shows that the iron is bound in the active site in a distorted trigonal bipyramidal coordination geometry, with Tyr447 and His462 located in the two axial positions and Tyr408, His460, and a solvent hydroxide located in the three equatorial positions (*4*, *5*). The X-ray crystal structure of the anaerobic PCA complex shows that the substrate chelates the iron such that the axial Tyr447 and the equatorial hydroxide are both displaced (*6*).

The proposed catalytic mechanism of 3,4-PCD is ordered sequential, with PCA binding prior to dioxygen (Scheme 1) (*1*, *2*, *6*). An important facet of this mechanism is the ability of the enzyme to undergo facile ligand rearrangements. Both

[†] This work was supported by National Institutes of Health Grants GM24689 (to J.D.L.) and GM46436 (to D.H.O.). M.P.V. was supported in part by NIH Training Grant GM08347.

[‡] The following PDB accession codes have been registered in the Protein Data Bank: 1YKK (mutant Y408C), 1YKL (Y408C + PCA), 1YKM (mutant Y408E), 1YKN (Y408E + PCA), 1YKO (mutant Y408H), and 1YKP (Y408H + PCA).

* To whom correspondence should be addressed. E-mail: lipsc001@umn.edu or Ohlen@umn.edu. Telephone: (612) 625-6454 (J.D.L.) or (612) 624-8436 (D.H.O.). Fax: (612) 624-5121.

[§] Current address: Promega Corp., 2800 Woods Hollow Road, Madison, WI 53711.

[∥] Current address: Laboratory of Structural Biology, National Institute of Environmental Health Sciences, P.O. Box 12233, Research Triangle Park, NC 27709.

[⊥] Current address: Department of Biochemistry, McGill University, 740 Dr. Penfield Ave., Montreal, Quebec H3A 1A4, Canada.

[#] Current address: Department of Biochemistry, Albert Einstein College of Medicine, 1300 Morris Park Ave., Bronx, NY 10461-1602.

[1] Abbreviations: PCA, protocatechuate; 4HB, 4-hydroxybenzoate; 3HB, 3-hydroxybenzoate; 4NC, 4-nitrocatechol; 3,4-PCD, protocatechuate 3,4-dioxygenase; RRT, reciprocal relaxation time.

10.1021/bi050902i CCC: $30.25
Published on Web 07/28/2005

Scheme 1: Catalytic Mechanism Proposed for 3,4-PCD

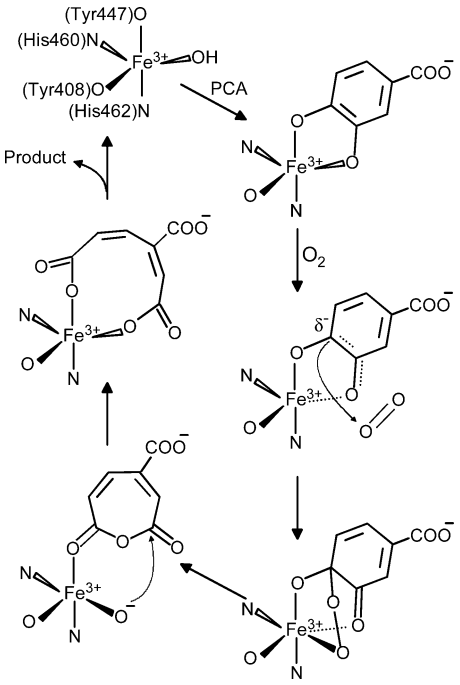

endogenous and exogenous ligands are required to bind and dissociate at different specific points in the catalytic cycle. On the basis of the X-ray crystal structures of a series of substrate and inhibitor complexes (*6*, *7*) and correlation with the optical properties of intermediates observed during the binding of PCA and inhibitors (*8*, *9*), it has been proposed that substrate initially binds in the hydrophobic active site pocket and subsequently displaces the equatorial OH^- ligand, resulting in a monodentate complex bound through the deprotonated 4-hydroxyl of PCA. The following step involves repositioning of the substrate to generate an octahedral coordination environment in which the PCA^{O4} is bound opposite Tyr408 and the equatorial ligand position opposite His460 is vacant. The formation of the chelate complex is thought to occur as the PCA^{O4} shifts to the axial ligand site and displaces Tyr447. This places the anionic PCA^{O4} ligand opposite a neutral His462 and allows the anionic Tyr447 to deprotonate the PCA 3-OH so that it can bind to the iron in the equatorial plane opposite Tyr408. This, in turn, creates an asymmetry in the PCA chelate structure with the shorter Fe−O bond formed with PCA^{O4} and serves to direct electrophilic attack by O_2 to PCA carbon 4. After carbon−carbon and oxygen−oxygen bond breakage and rearrangement, protonation and release of the product are also likely to involve the sequential dissociation of two carboxylates and the return of Tyr447 and a solvent hydroxide to their positions in the resting state enzyme. All of these coordination changes require that the exchange rates of the ligands involved exceed the turnover number for the enzyme. The mechanism used by nature to facilitate these high exchange rates is one topic of this report.

The mechanism shown in Scheme 1 predicts that Tyr447 will exert its greatest influence on the substrate binding and product release steps because it is dissociated during the actual O−O bond-breaking and insertion steps of the cycle. Accordingly, site-directed mutation of this residue resulted in an enzyme that binds substrate and releases products 100−1000 times slower than wild type but allows the O_2 binding and reaction steps to proceed nearly unchanged (*10*). In contrast to Tyr447, the remaining three endogenous ligands are not displaced from the iron and could potentially influence steps throughout the catalytic cycle through Lewis basicity and trans ligand effects. This is particularly true of the anionic Tyr408 ligand which is located opposite the substrate binding cavity where it could contribute to the lability of several ligands throughout the catalytic cycle, namely, the OH^- in the resting state, both the 4-O^- and 3-O^- of PCA during the binding process, and one or both of the product carboxylates during the product dissociation process.

To explore the roles of Tyr408 during 3,4-PCD catalysis, this residue has been mutated to His, Glu, Phe, and Cys, and the resulting enzymes have been structurally, spectroscopically, and kinetically characterized. For each of these mutants, it is found that the new residue at position 408 can no longer directly coordinate to the active site iron. Nevertheless, significant differences in the spectroscopic and kinetic properties of the various mutant enzymes are noted. These changes are found to be consistent with the proposed mechanistic roles for Tyr408, but they also provide insight into the profound effects of second-sphere amino acid residues on catalysis.

EXPERIMENTAL PROCEDURES

Chemicals and Standard Procedures. All chemicals, except where noted, were obtained from Sigma or Aldrich Inc. Enzyme grade ammonium sulfate for crystallization was purchased from ICN Biomedicals Inc. PCA was recrystallized and dried under vacuum. Anaerobic sample handling techniques were performed as previously described (*11*).

Site-Directed Mutagenesis. The techniques used for cloning and plasmid manipulation were previously described (*10*, *12*). All mutations were created in pRWF120, a modified version of pALTER-1 containing a 300 bp *Sal*I−*Bst*EII fragment of *pcaHG* from *P. putida* (ATCC 23975), using the "Altered Sites" kit purchased from Promega Inc. and the oligonucleotides listed in Table 1. All restriction endonucleases and modifying enzymes were purchased from New England Biolabs, Promega, and GIBCO BRL (Life Technologies). DNA sequencing was performed by the Microchemical Facility at the University of Minnesota. For expression in *Pseudomonas fluorescens*, the *Sal*I−*Bst*EII fragment containing the Y408E mutation was cloned into pRWF115, a modified version of pALTER-1 containing the complete *pcaHG* genes. The mutant Y408E genes were then subcloned into the broad-host range expression plasmid pKMY319 to generate pRWF210. For expression in *Escherichia coli* BL21(DE3), the *Sal*I−*Bst*EII fragments containing Y408C, Y408F, and Y408H mutations were cloned directly into pCE120, a pT7-7 expression plasmid containing the complete *pcaHG* genes, yielding pCE014, pCE022, and pCE012.

Growth and Expression. *P. fluorescens* containing pRWF210 was grown as previously described (*10*, *12*) but scaled up to a 240 L fermentor in the Biological Process Technology Institute at the University of Minnesota. *E. coli* BL21(DE3) containing pCE012, pCE014, or pCE022 were grown from fresh heat-shock transformations, and colonies were used to directly inoculate 1 L of Luria broth (LB) at 600 μg/mL ampicillin, 1% glucose, and 37 °C. When the

Table 1: Oligonucleotides Used for Generation of Site-Directed Mutations of 3,4-PCD

	oligonucleotide primer[a]	expression plasmid
Y408H	5′-CAACGCCGGTGGCCGCCACCGGCACAAGAACGAC-3′	pCE012
Y408E	5′-CAACGCCGGTGGCCGCGAGCGGCACAAGAACGAC-3′	pRWF210
Y408C	5′-CAACGCCGGTGGCCGCTGCCGGCACAAGAACGAC-3′	pCE014
Y408F	5′-CAACGCCGGTGGCCGCTTCCGGCACAAGAACGAC-3′	pCE022

[a] Nucleotides encoding the 408 residue are underlined.

optical density at 600 nm reached 0.8, 200 mL of the starter culture was used to inoculate 10 L of 2× LB in a Microferm fermentor (New Brunswick Scientific Co., Inc., Edison, NJ) at 600 μg/mL ampicillin, 2% glucose, and 37 °C. The fermentor was maintained at pH = 7.0 using 7.5 M NH_4OH and monitored for glucose using reagent strips purchased from Boehringer Mannheim Corp. and, upon glucose depletion, induced with 1 mM IPTG at 30 °C. After 3 h of induction, cells were harvested in a Beckman JA-10 rotor at 9000 rpm for 15 min and stored at −80 °C.

Purification. All purification steps were performed at 4 °C, and all column resins were purchased from Pharmacia Biotech. Frozen *E. coli* cell paste (100−200 g) was resuspended in 300 mL of buffer B (20 mM Tris, pH 8.5, 2 mM β-mercaptoethanol), disrupted by sonication, and centrifuged in a Beckman JA-17 rotor at 17000 rpm for 90 min. The cell-free extract was directly loaded onto a 300 mL DEAE-Sepharose Fast Flow column (5.5 × 19 cm), preequilibrated with buffer B, and washed with 1.0 L of 75 mM NaCl in buffer B. Protein was eluted in a linear gradient (1.5 L of 75 mM NaCl in buffer B × 1.5 L of 300 mM NaCl in buffer B) at a rate of 2 mL/min. Due to the low activity of the mutant enzymes, fractions from all columns were pooled on the basis of the presence of the bands from the α and β subunits on an SDS−polyacrylamide gel using the PhastGel System from Pharmacia Biotech and comparison with previously purified wild-type enzyme. The DEAE pool was adjusted to 0.8 M $(NH_4)_2SO_4$ and loaded onto a 300 mL phenyl-Sepharose CL-4B column (4.5 × 22.5 cm), preequilibrated with 0.8 M $(NH_4)_2SO_4$ in buffer A (50 mM Tris, pH 8.5, 2 mM β-mercaptoethanol), and washed with 500 mL of 0.8 M $(NH_4)_2SO_4$ in buffer A. Protein was eluted in a linear gradient [1.5 L of 0.8 M $(NH_4)_2SO_4$ in buffer A × 1.5 L of buffer A] at a rate of 2 mL/min. Fractions from the phenyl column were pooled and concentrated to less than 10 mL using a 350 mL Amicon concentrator with a 76 mm YM-100 membrane at 10 psi and then loaded onto a 500 mL Sephacryl S-300 column (3 × 97.5 cm), preequilibrated with buffer A. Pure fractions eluted with buffer A at a rate of 1 mL/min and were concentrated with Centricon-100s (Amicon) in a Beckman JA-20 at 3000 rpm. Enzyme from *P. fluorescens* was purified as previously described (*10*, *12*). Each enzyme purification yielded a single visible band for each subunit after SDS−PAGE separation and silver staining.[2]

Iron Reconstitution. All solutions were maintained under anaerobic conditions. Six milliliters of 100 mM Tris, pH 8.5, was added to 52 mg of $Na_2S_2O_4$, and 4 mL of this solution was added to 78 mg of $Fe(NH_4)_2(SO_4)_2$ to generate a final solution 50 mM in each. Two milliliters of the reduced iron solution was added to 1 mL of concentrated enzyme (<2 mM) and allowed to mix anaerobically for ≥4 h. A 100 mL Sephadex G-25 column (3 × 25 cm; Pharmacia Biotech) was equilibrated with buffer A that had been deoxygenated by bubbling with N_2, and the iron−enzyme mixture was quickly loaded. Reconstituted protein eluted with buffer A at a rate of 1 mL/min and was concentrated as before.

Atomic Absorption Spectroscopy. Iron was quantitated from a known amount of protein using a Varian SpectrAA-100 flame atomic absorption spectrometer at 248.3 nm. Standards were prepared from a 1000 ppm iron solution purchased from Aldrich and diluted with 1−2% nitric acid to a working range of 1−15 ppm.

Absorption Spectroscopy and Kinetics. All spectra were recorded on a GBC UV/vis 920 spectrophotometer. Enzyme concentrations were determined using ϵ(280 nm) = 1.32 mL/mg. Enzyme assays typically contained 200 μM PCA and 250 μM oxygen in 50 mM Tris at pH = 8.5 using $\Delta\epsilon$(290 nm) = 2300 M^{-1} cm^{-1}, the difference between PCA (ϵ = 3800 M^{-1} cm^{-1}) and product (ϵ = 1500 M^{-1} cm^{-1}). Due to the low mutant activity, steady-state PCA turnover was measured at 25 °C. The transient binding of substrates and inhibitors was monitored at single wavelengths between 400 and 700 nm at 4 or 25 °C using an Applied Photophysics SX.18.MV stopped-flow spectrophotometer. Diode array spectra were recorded using the same instrument. The exponential decay curves were fit by nonlinear regression using the program KFIT, and numerical integration simulations were performed using KSIM (both programs from Neil Millar, Kings College, London).

In a reversible two-step binding reaction in which the first step involves ligand association with the enzyme (k_1 and k_{-1}) and the second involves a conformational change or the actual binding of the ligand to the iron (k_2 and k_{-2}), the first step may be much faster than the second. In this case, one often observes only the slower of what is actually a two-phase time course. The ligand concentration dependence of this second phase can be fit to the equation (*9*, *13*):

$$1/\tau_2 = k_{-2} + k_{+2}[L]/(K_1 + [L]) \quad (1)$$

where τ_2 is the observed relaxation time, [L] is the ligand concentration, k_{+2} and k_{-2} are the forward and reverse rate constants of the second step, and K_1 is the dissociation constant of the initial complex between the enzyme and the ligand ($K_1 = k_{-1}/k_{+1}$). If K_1 is much smaller than the working ligand concentration, the equation becomes ligand independent, $1/\tau_2 = k_{-2} + k_{+2}$, and K_1 cannot be determined. If this is not the case, then both K_1 and the overall dissociation constant (K_d) can also be calculated: $K_d = K_1/(1 + k_{+2}/k_{-2})$.

[2] Recombinant 3,4-PCDs with mutations at position 408 did not express as well as the recombinant wild-type enzyme. The Y408E mutant was expressed so poorly that it could not be detected in *E. coli* cells and could only be purified from *P. fluorescens*. Consequently, insufficient Y408E protein was obtained for resonance Raman and kinetic experiments.

The dissociation constants for tight binding inhibitors were determined using a competition titration method (*9*). First, the $K_{d(3HB)}$ for the weak inhibitor 3-hydroxybenzoate (3HB) was determined by monitoring changes in the optical absorption spectrum of 3,4-PCD upon addition of increasingly concentrated aliquots of 3HB. The $K_{d(3HB)}$ can be calculated according to the equation:

$$[I]_b = [E]_t[I]_f/(K_d + [I]_f) \quad (2)$$

where $[I]_b$ is the concentration of bound inhibitor, $[I]_f$ is the concentration of free inhibitor, and $[E]_t$ is the total enzyme concentration. For the tight binding inhibitor 4-hydroxybenzoate (4HB), the amount of enzyme required for an optical titration (~50−100 μM) was greater than the $K_{d(4HB)}$. At inhibitor concentrations below $[E]_t$, $[I]_f$ was essentially zero, and the data could not be accurately fit to a hyperbola. However, in the presence of 3HB, the bound concentration of 4HB was dependent on the bound concentration and dissociation constant of 3HB. This generated a hyperbola with an apparent $K_{d(4HB)}$ greater than $[E]_t$. When 3HB is in large excess (30 mM), $[E]_t = [3HB]_b$, and absorbance changes upon titration with 4HB illustrate the gradual conversion of $[3HB]_b$ to $[4HB]_b$. The real $K_{d(4HB)}$ was then calculated using the equation:

$$\frac{[4HB]_b}{[3HB]_b} = \frac{K_{d(3HB)}[4HB]_f}{[3HB]_t K_{d(4HB)}} \quad (3)$$

where $[3HB]_t$ and $[4HB]_f$ are the total and free inhibitor concentrations and $[4HB]_b/[3HB]_b$ is the ratio of bound inhibitors. Throughout this study, unless otherwise stated, K_d refers to the overall dissociation constant.

Crystallization and X-ray Diffraction. All solutions were sterile filtered, and enzyme was centrifuged at 18000*g* for 5 min to remove precipitates. Crystals of mutant 3,4-PCD were grown at 4 °C by hanging drop vapor diffusion by placing 2 + 2 μL droplets of 20−40 mg/mL protein against 1.6−1.8 M $(NH_4)_2SO_4$, 100 mM Tris, pH 8.5, and 2 mM 2-mercaptoethanol. For substrate complexes, aerobically grown crystals were transferred to a Coy anaerobic tent, mounted, and then washed with anaerobic 30 mM PCA solution in mother liquor until a slight color change was observable (typically at 30 min). X-ray diffraction data were collected at room temperature on a Siemens area detector or an R-Axis IV imaging plate system using Cu Kα radiation generated by a Rigaku RU-200B rotating anode. Data from the Siemens detector were processed using XENGEN (*14*); data from the R-Axis IV were processed using CRYSTALCLEAR [Molecular Structure Corp. (*15*)]. Structural models were examined using O (*16*) and refined using CNS (*17*). The initial model for refinement was derived from the wild-type 3,4-PCD structure in which all solvent molecules in the active site were removed and Tyr408 was replaced by the substituted amino acid. Next, additional active site solvent molecules, the 2-mercaptoethanol modification at Cys429S, and either (i) a solvent molecule, (ii) a SO_4^{2-} molecule, or (iii) a CO_3^{2-} molecule coordinated to the iron were added to the model, consistent with the electron density maps. There were no iron−ligand bond distance restraints during the refinements. The stereochemical quality of the final model (see Table 2 in Results) was assessed with WHATCHECK (*18*) and PROCHECK (*19*). Figures 1 and 2 were prepared with SPOCK (*20*). All X-ray crystal structure figures were produced with PyMOL (DeLano Scientific LLC, South San Francisco, CA).

Resonance Raman Spectroscopy. Spectra were collected on an Acton AM-506 spectrometer (2400-groove grating) using a Kaiser Optical holographic supernotch filter with a Princeton Instruments liquid N_2-cooled (LN-1100PB) CCD detector with 4 cm^{-1} spectral resolution. Spectra were obtained by scattering from a 100 μL sample in a spinning cell cooled with a flow of 0 °C nitrogen gas. Laser excitation wavelengths from 457.9 to 632.8 nm were generated from a Spectra Physics 2030-15 argon laser and a 375B CW dye (rhodamine 6G). Raman frequencies were referenced to indene. Baseline corrections were performed using Grams/32 Spectral Notebase (Galactic). 4-[^{18}O]Hydroxybenzoate was synthesized as previously described (*21*).

RESULTS

Mutant Expression, Purification, and Iron Reconstitution. Wild-type and mutant 3,4-PCDs with Phe, Cys, His, and Glu residues replacing Tyr408 were expressed in recombinant *E. coli* or *P. fluorescens* strains and purified to homogeneity as described in Experimental Procedures.[3] Overexpression in *E. coli* resulted in enzyme with only about one-third of the 12 active sites occupied by Fe(III). Reconstitution with Fe(II) under reducing anaerobic conditions, followed by removal of excess iron and subsequent oxidation, increased the iron occupancy for most of the recombinant enzymes to about 10 sites per dodecamer, comparable to that found for 3,4-PCD purified from the native source (*12*). The iron in the mutant enzymes was tightly bound except in the case of the Y408F mutant, which did not reconstitute above half-occupancy and lost color during crystallization attempts, implying loss of bound iron. Thus, only Y408C, Y408H, and Y408E were crystallized for X-ray diffraction studies.

X-ray Crystal Structures. The X-ray crystal structures of the mutant 3,4-PCD enzymes Y408H, Y408E, and Y408C were determined with and without substrate bound as described in Experimental Procedures. The crystal parameters and structural statistics are summarized in Table 2. Relevant distances in the vicinity of the active site iron are listed in Table 3. As shown in Figure 1, the structures reveal no significant mutation-related changes except in the immediate vicinity of the altered amino acid (rmsd over all atoms = 0.2−0.3 Å). In particular, the positions of the other endogenous iron ligands are either unaltered or only slightly shifted. The position of the peptide backbone in the vicinity of the iron is essentially unaffected in each structure, even in the case of the altered amino acid. Consequently, none of the new amino acids were found to coordinate to the iron because the side chains are shorter than that of Tyr in each case. As shown in Figures 1 and 2 and Table 3, the newly vacant ligand site in each mutant is occupied by a solvent. The solvent to iron distance is different for each mutant, becoming

[3] A Y408A mutation was also constructed, expressed, and partially purified but proved to be unstable. A single growth and purification in *P. fluorescens* yielded a total of only 0.25 mg, so this mutation was not pursued. However, a LMCT band at 525 nm was observed in the resting Y408A enzyme analogous to those observed in the other mutants.

Table 2: X-ray Crystal Structure Determination Statistics and Parameters

	Y408C	Y408C + PCA	Y408E	Y408E + PCA	Y408H	Y408H + PCA
Data Collection						
PDB ID	1YKK	1YKL	1YKM	1YKN	1YKO	1YKP
resolution cutoff	2.3	2.3	2.3	2.3	2.3	2.3
*I*2 unit cell [*a*, *b*, *c* (Å); β (deg)]	194.9, 127.0, 132.8; 96.4	196.7, 127.2, 133.9; 97.6	196.6, 127.7, 134.3; 97.7	195.8, 128.6, 134.4; 98.0	196.6, 127.6, 134.5; 97.6	196.2, 128.0, 134.2; 97.7
total observations (unique)	137248	144055	105279	116391	82448	91484
R_{merge}	12.4	14.6	13.9	25.9	14.1	19.4
Model Refinement						
resolution range (Å)	50−2.3	50−2.3	50−2.3	50−2.3	50−2.3	50−2.3
R_{free} (%)	22.34	21.72	19.81	18.53	21.97	20.87
R-factor (%)	19.45	15.34	16.65	13.20	18.51	14.58
rmsd from ideal 23 symmetry (Å)	0.3371	0.3085	0.2178	0.2784	0.1632	0.2584
no. of non-hydrogen protein atoms	20664	20640	20682	20682	20688	20701
no. of solvent O atoms	792	996	1314	1512	750	780
mean *B* values (Å^2)						
α subunit	39.410	36.479	26.785	23.124	30.121	29.842
β subunit	32.987	29.982	20.430	17.520	23.903	24.146
substrate		62.899		54.202		92.484

Table 3: Selected Interatomic Distance in the Crystal Structures of 3,4-PCD Tyr408 Mutants

distance or angle	Y408C	Y408C + PCA	Y408E	Y408E + PCA	Y408H	Y408H + PCA
$Y408(X)^{X4}$−Fe (Å)			3.6	3.9	3.9	3.8
$Y447^{O4}$−Fe (Å)	2.0	2.2	2.1	2.5	2.1	2.4
$H460^{N\epsilon2}$−Fe (Å)	2.3	2.5	2.3	2.4	2.5	2.4
$H462^{N\epsilon2}$−Fe (Å)	2.2	2.4	2.1	2.3	2.2	2.6
$solvent^{408}$−Fe (Å)	2.4	3.1	2.2	2.5	2.0	2.4
solvent/PCA^{O4}−Fe (Å)	3.2	2.6	3.1	2.3	3.0	2.0
$Y408(X)^{X4}$−$solvent^{408}$ (Å)	2.9	2.4	2.6	2.4	2.6	2.2
$Y447^{O4}$−Fe−$H460^{N\epsilon2}$ (deg)	105.65	96.97	92.03	87.62	89.38	87.38
$Y447^{O4}$−Fe−$H462^{N\epsilon2}$ (deg)	151.37	173.46	172.79	176.73	172.45	174.34
$Y447^{O4}$−Fe−$solvent^{408}$ (deg)	98.62	82.58	93.1	85.15	100.61	98.2
$Y447^{O4}$−Fe−solvent/PCA^{O4} (deg)	51.47	51.39	74.86	61.05	77.18	60.97
$H460^{N\epsilon2}$−Fe−$H462^{N\epsilon2}$ (deg)	88.63	87.13	94.33	95.01	85.57	88.84
$H460^{N\epsilon2}$−Fe−$solvent^{408}$ (deg)	116.07	113.8	90.04	90.87	82.46	98.09
$H460^{N\epsilon2}$−Fe−solvent/PCA^{O4} (deg)	84.79	90.39	99.64	87.41	101.75	105.95
$H462^{N\epsilon2}$−Fe−$solvent^{408}$ (deg)	96.97	100.47	90.29	96.74	84.31	86.5
$H462^{N\epsilon2}$−Fe−solvent/PCA^{O4} (deg)	107.08	123.75	100.68	117.05	98.34	116.24

longer in the order Y408H < Y408E < Y408C. In the case of Y408C (Figure 2), the electron density is continuous between the iron and the new Cys408 over a distance of ∼5 Å, suggesting that at least two new solvents occupy this space. The electron density indicates that the Cys408 residue can occupy two positions with equal occupancy by rotation around the Cα−Cβ bond, suggesting that there is no strong interaction to orient the sulfur. The new Glu408 and His408 are each well oriented, and the potentially bonding Oϵ and Nϵ atoms are located 3.63 and 3.85 Å from the iron, respectively, with only a single solvent required to fit the density between the new amino acid and the iron. In the case of Y408H, this density is both less well resolved and less than 2 Å from the iron. This suggests that the new solvent ligand is strongly hydrogen bonded to His408 such that it is bound to the iron with significant OH^- character. In contrast, the best placement of the closest solvent in the case of Y408C is 2.45 Å from the iron, suggesting that this solvent is bound as water.

The equatorial solvent in the substrate binding pocket side of the Fe(III) ligation of wild-type 3,4-PCD is present in each of the mutant structures. In the case of the Y408C mutant, it is slightly closer to the iron than in the other mutants and shifted to be opposite the solvent that replaces Tyr408 to establish nearly octahedral coordination symmetry with one missing equatorial ligand.

Upon anaerobic PCA binding, the active site solvent in each of the mutant 3,4-PCDs is displaced as observed for the wild-type enzyme. However, in contrast to the wild-type enzyme, Tyr447 remains bound to the iron in each mutant enzyme complex as illustrated in Figures 1 and 3A. As a result, a monodentate substrate complex is formed between the iron and PCA^{O4}. This bond ranges from 2.15 Å in the case of Y408H to 2.60 Å for Y408C with a large range of distances (±0.35 Å) exhibited in the six protomers of the asymmetric unit. The origin of this distance distribution is not clear, but a bond to the iron is apparent in each case. In contrast, the PCA^{O3} is >3.7 Å from the iron for each mutant enzyme complex, and thus this group is not ligated. The bond from the PCA^{O4} to the iron is longer in each case than that of the same bond in the wild-type enzyme (1.9 Å). However, the PCA is bound in the mutant complexes in a completely different orientation, with the PCA^{O4} ligating in an equatorial rather than axial position. In fact, the aromatic ring and O4 group of PCA in the mutant enzyme complexes nearly superimpose on those of 4-hydroxybenzoate (4HB) in its complex with the wild-type enzyme (Fe−$4HB^{O4}$ bond length = 2.2 Å) (*7*). This complex is thought to mimic a step in the substrate binding sequence before the final substrate iron chelate forms. Thus, PCA binding in the mutant enzymes appears to proceed only partway through the sequence, arresting at the penultimate binding step.

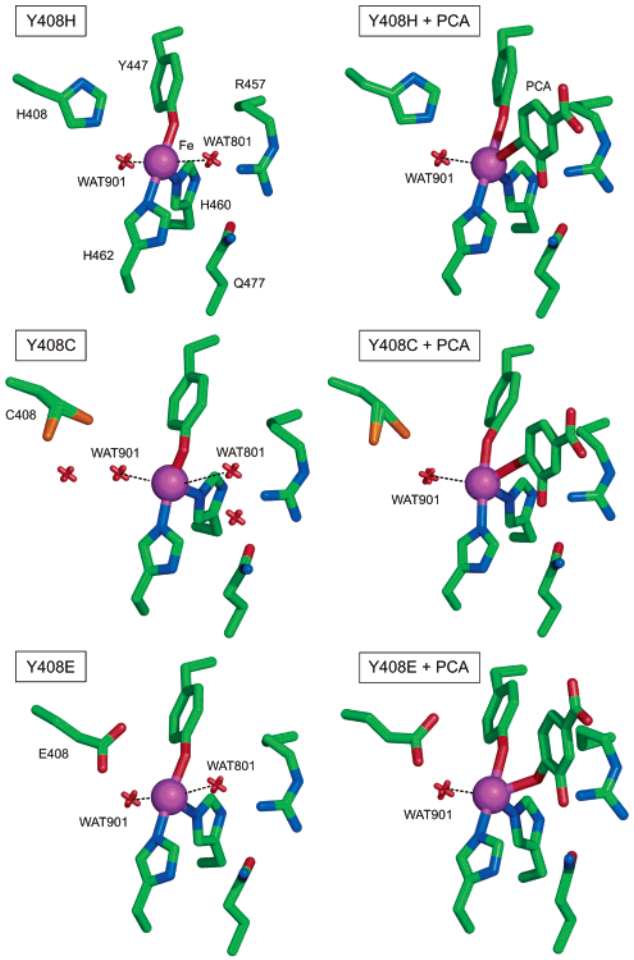

FIGURE 1: X-ray crystal structures of the active site region of the 3,4-PCD mutants with and without PCA. Solvents 801 (substrate pocket) and 901 (between iron and mutated residue 408) are within bonding distance to the iron (dashed lines).

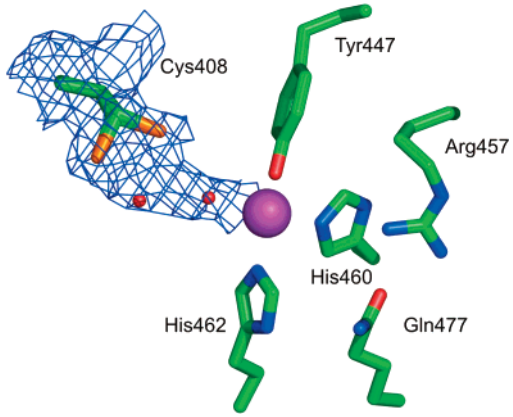

FIGURE 2: X-ray crystal structure of the active site region of Y408C showing continuous electron density between the sulfur of Cys408 and the iron via intervening solvents.

The iron atom shifts slightly in position as the position 408 residue changes as shown in Figure 3. In the PCA complexes, there is very little movement of the iron along the axial ligand axis. However, in the Y408C−PCA complex, the iron shifts about 0.5 Å in the equatorial plane away from the substrate binding site, while the shift is about half as large in the Y408E−PCA complex and no shift is seen for Y408H−PCA. In each of the mutant enzymes, both of the axial ligands move slightly toward the position formerly

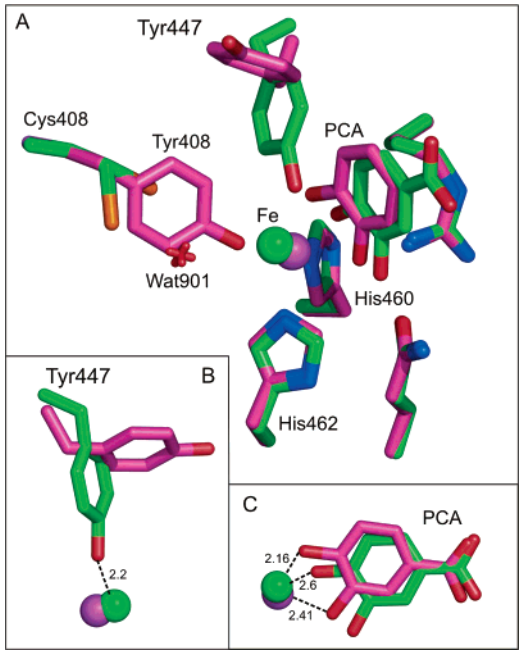

FIGURE 3: Overlay of the X-ray crystal structures of the active site regions of the Y408C (green) and wild-type 3,4-PCD (magenta) complexes with PCA (A). The PCA carboxylate for the latter structure is omitted for clarity. (B) Comparison of the positions of the axial Tyr447. (C) Comparison of the PCA orientations. Distances are shown in angstroms. The distance between the iron and PCA^{O3} in the Y408C−PCA complex is 3.75 Å, suggesting that it is not bound.

occupied by Tyr408 due to a decrease in bulk at this position. This typically results in a lengthening of the residue's bond to the iron, an effect which is most significant in the case of the Y408E and Y408H mutants where the $Tyr447^{O\eta}$−Fe bond is increased about 0.2 Å relative to the wild-type enzyme complex. The $Tyr447^{O\eta}$−Fe bond is unchanged in the case of the Y408C mutant where the shift in the iron position compensates for the shift in the axial ligand positions. The same general trend toward longer ligand bonds is also observed for the PCA complexes of the mutant enzymes, with the axial ligand bonds lengthening slightly compared with the substrate-free molecules in all cases.

4-Nitrocatechol Complex. Perhaps the most unexpected findings from the crystal structures of the 3,4-PCD mutants are the failure of PCA to shift into a chelated orientation and the failure of Tyr447 to dissociate. In the proposed mechanism of 3,4-PCD, these are fundamental steps in preparing the substrate to react with O_2. The crystal structure does not provide a rationale for these observations. However, these steps are tightly coupled in the substrate activation mechanism because the dissociated Tyr447 is proposed to be the base that deprotonates PCA from the monoanion to the dianion so that it can form a strong chelate. This can be examined for the mutant enzymes using the substrate analogue and competitive inhibitor 4-nitrocatechol (4NC) because its optical features change dramatically as the OH groups deprotonate (Figure 4A−C) (*22*, *23*). The high affinity of 4NC for 3,4-PCD allows a nearly stoichiometric complex to be formed that exhibits a spectrum characteristic of the dianionic state for the wild-type enzyme as expected (Figure 4D). In contrast, the stoichiometric complexes of 4NC with the mutant enzymes elicit spectra with a single band at 440 nm characteristic of the monoanionic form (Figure 4E). This

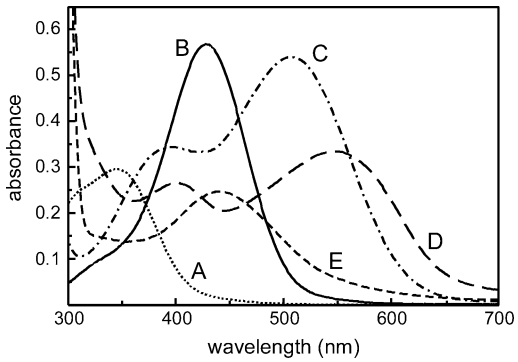

FIGURE 4: Optical absorption spectra of 4-nitrocatechol and complexes with 3,4-PCD. All samples contain 50 μM 4NC. (A) Fully protonated form, 100 mM MES, pH 4.0. (B) Monoanionic form, 50 mM Tris, pH 8.5. (C) Dianionic form, 100 mM CAPS, pH 12.0. (D) 50 mM Tris, pH 8.5, plus 50 μM [Fe(III) sites] wild-type enzyme. (E) 50 mM Tris, pH 8.5, plus 50 μM [Fe(III) sites] Y408C enzyme. 4NC complexes with the other 408 mutants yield spectra identical to (E).

shows that only one of the 4NC hydroxyls is deprotonated in these complexes and is consistent with the lack of the in situ active site base that would be provided by dissociating Tyr447.

Absorption Spectra. The burgundy color of the wild-type enzyme, with a peak at 450 nm and a shoulder around 500 nm, is due to ligand-to-metal charge transfer (LMCT) between the tyrosinate ligands and the Fe(III) (*24*). Early resonance Raman (*25*) and more recent CD/MCD and theoretical studies (*26*) of wild-type *Brevibacterium fuscum* 3,4-PCD have demonstrated individual LMCT transitions at about 331, 440, and 568 nm for the equatorial tyrosine (analogous to Tyr408) and 314, ~380, and 485 nm for the axial tyrosine (analogous to Tyr447). Mutation of Tyr408 shifts the absorption maximum of the enzyme to 500−520 nm and creates a more symmetrical peak (Figure 5, solid lines), consistent with the loss of the Tyr408 LMCT bands.

The binding of PCA to the wild-type and mutant 3,4-PCDs leads to new absorption bands consistent with the presence of an additional catecholate or phenolate ligand (Figure 5, dashed lines). Because these substrate complexes exhibit such broad absorption spectra, it is difficult to assign wavelengths to individual ligands. However, since the crystal structures show that Tyr447 is bound in each case that was investigated (there is no structure for Y408F) and each spectrum exhibits absorbance in the 500 nm region, it is likely that Tyr447 continues to contribute a band in this region. If this is the case, then the difference spectra before and after addition of PCA, an example of which is shown in Figure 6, can be used to determine the approximate position of the new band-(s). The energy of this new absorption band is different for each mutant, gradually increasing in the order Y408F ≈ Y408C < Y408E < Y408H (Table 4). The PCA complexes of the Y408C and Y408F mutants exhibit the broadest optical bands, due to the widely separated contributions from the substrate and Tyr447 LMCT bands. In contrast, these bands have much more similar energies for the Y408H−PCA complex. The binding of the competitive inhibitor 4HB also produces an increase in absorption for the wild-type and mutant enzymes, with the position of the inhibitor LMCT absorption band blue shifted with respect to the substrate LMCT band from the PCA complex in each case (Figures 5 and 6, dotted lines). Nevertheless, the same mutation-specific energy pattern is observed such that the energy of the LMCT bands due to 4HB are ordered with Y408F ≈ Y408C < Y408E < Y408H (Table 4).

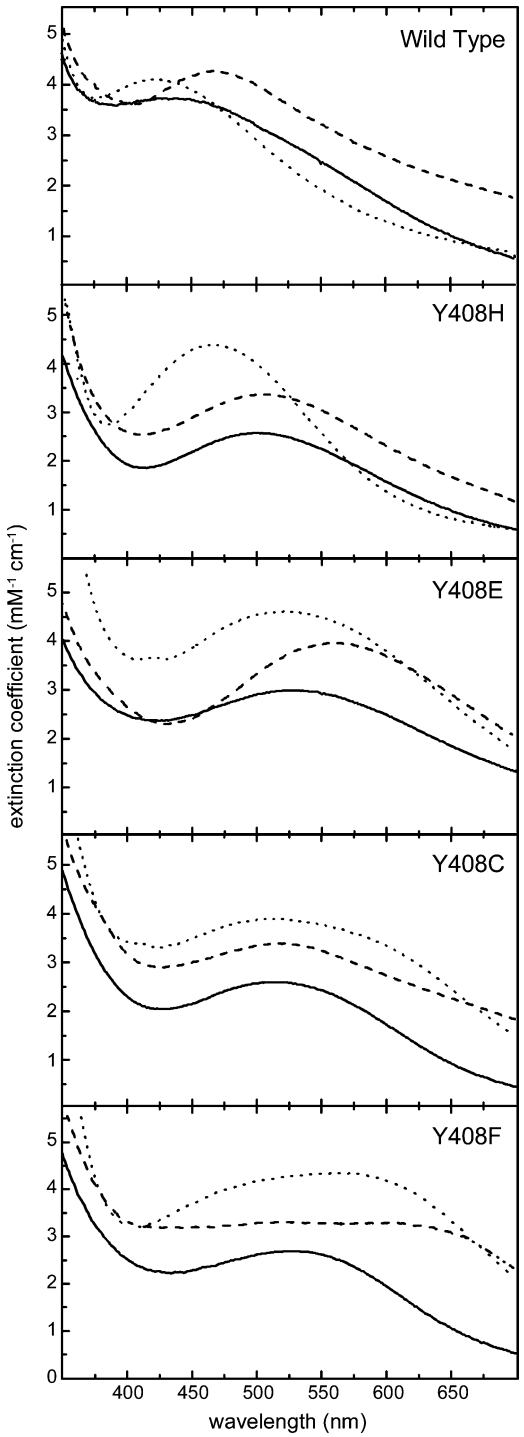

FIGURE 5: Optical absorption spectra of wild-type and mutant 3,4-PCDs. Samples were prepared in 50 mM Tris and 2 mM β-mercaptoethanol, pH 8.5, with enzymes (100 μM) in the resting state (solid lines) and bound with 2 mM PCA (dashed lines) or 2 mM 4HB (dotted lines).

The absorption spectra were used to determine the approximate K_d values for the inhibitor and PCA complexes (see Experimental Procedures) and are listed in Table 5. Inhibitors such as 4HB and 3HB were found to bind more tightly to the mutant enzymes, whereas the substrate PCA binds less tightly. The latter observation is in accord with

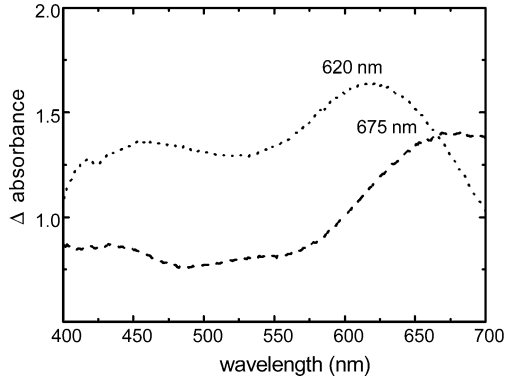

FIGURE 6: Difference spectra for Y408C. The absorption spectrum of the resting enzyme was subtracted from the spectrum of the PCA complex (solid line) or the 4HB complex (dotted line) shown in Figure 5.

Table 4: Absorption Maxima (nm) of LMCT Bands Determined by Difference Spectra

	PCA	4HB
Y408H	525	450
Y408E	600	500
Y408C	675	620
Y408F	675	625

Table 5: Inhibitor and Substrate Dissociation Constants (μM) Determined by Optical Titration at 25 °C[a]

	3HB	4HB	PCA
wild type	3500	300	2.5[b]
Y408H	180	6.3	39
Y408E	210	nd[c]	nd[c]
Y408C	2500	51	57
Y408F	1800	12	nd[c]

[a] The experiments were conducted as described in Experimental Procedures. Errors are ±10%. [b] From ref *33*. [c] Not determined.

the data presented here indicating that the substrate does not bind in the same way to the wild-type and mutant enzymes. The monodentate binding of PCA to the mutant enzymes is evidently weaker than chelate binding, although it is still 10−100-fold stronger than the binding of monodentate inhibitors to the wild-type enzyme. Because the monohydroxy inhibitors bind to form a monodentate complex in both the wild-type and mutant enzymes, a more valid comparison can be made and reveals the higher inherent affinity of the mutant enzymes.

Resonance Raman Spectroscopy. Resonance Raman spectroscopy can be used to more extensively characterize the phenolate to iron LMCT bands of 3,4-PCD (*27*−*30*). The high-energy region of the spectrum of the Y408C mutant is shown in Figure 7A, and the spectroscopic features for each of the mutants are summarized in Table 6. Previous studies have shown that, upon addition of 4HB to the wild-type enzyme, three ν C−O/7a vibrations (nomenclature taken from ref *31*) around 1300 cm^{-1} can be observed, one from each tyrosine and one from bound inhibitor (*25*). When 4HB is added to the mutant enzymes, only two ν C−O/7a vibrations are resolved, consistent with the absence of Tyr408. The chromophores giving rise to these transitions can be identified on the basis of their excitation profiles. In the profile of the Y408H mutant, both vibrations are most intense with 550 nm excitation, indicating that very similar

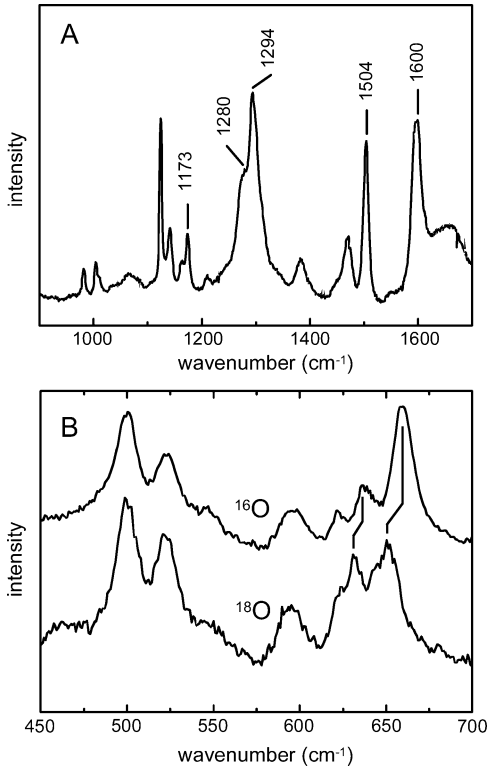

FIGURE 7: Resonance Raman spectra of the Y408C mutant bound with 4HB. 750 μM enzyme was prepared in 50 mM Tris and 2 mM β-mercaptoethanol, pH 8.5, with either 15 mM ^{16}O-4HB or 3 mM ^{18}O-4HB. High- (A) and low- (B) energy vibrations were generated with an excitation wavelength of 514.5 nm. Vibrations characteristic of iron−phenolate coordination are marked in the high-energy region. The upper and lower spectra in (B) are complexes with ^{16}O- and ^{18}O-4HB, respectively. Peaks that shift upon isotopic labeling are marked.

Table 6: Resonance Raman Features (cm^{-1})[a]

	ν Fe−O	δ C−H	ν C−O/7a	ν C−C
wild type	587, 641	1171	1257, 1276, 1287	1503, 1604
Y408H	595, 643	1175	1306, 1311	1507, 1603
Y408C	598, 660[b]	1173	1280, 1294	1504, 1600
Y408F	597, 657[b]	1174	1276, 1297	1504, 1600

[a] Nomenclature from ref *31*. [b] Additional vibrations are observed in the Y408C and Y408F mutants at 637 and 640 cm^{-1}, respectively, that shift upon isotopic labeling.

absorption band energies are associated with Tyr447 and 4HB (Figure 8) in accord with the interpretation of the absorbance spectra described above. In the profiles of the Y408C and Y408F mutants, the lower energy vibration also maximizes with 550 nm excitation, but the higher energy vibration is most intense with excitation above 650 nm (Figure 8). The excitation profile for the lower energy vibration is similar for the wild-type enzyme and each of the mutants. This allows assignment of the lower energy vibration to the Tyr447$^{O\eta}$−Fe interaction and the higher energy vibration to the 4HB^{O4}−Fe interaction.

The lower energy region of the resonance Raman spectrum (450−700 cm^{-1}) contains information about the metal−ligand bonds (the spectrum for the Y408C mutant is shown in Figure 7B). Again, these bands are commonly observed for enzymes with iron−phenolate coordination. In particular, the vibration around 590 cm^{-1} is often present, and density functional calculations assign it to be a ν Fe−O transition

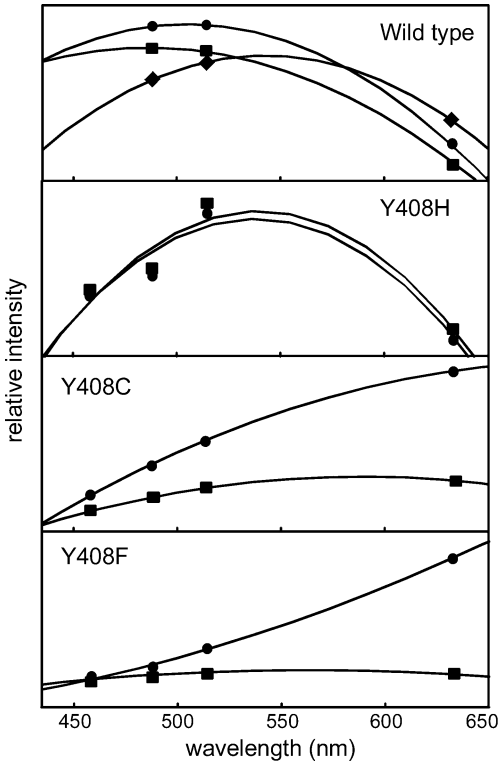

FIGURE 8: Resonance Raman excitation profiles of 3,4-PCD bound with 4HB. The intensity of each ν C−O/7a vibration is relative to the ammonium sulfate peak at 983 cm^{-1}, and the energy of each vibration is as follows: wild-type vibrations are located at 1257 cm^{-1} (■), 1276 cm^{-1} (●), and 1287 cm^{-1} (◆); Y408H vibrations at 1306 cm^{-1} (■) and 1311 cm^{-1} (●); Y408C vibrations at 1280 cm^{-1} (■) and 1294 cm^{-1} (●); and Y408F vibrations at 1276 cm^{-1} (■) and 1297 cm^{-1} (●). Solid lines show second-order polynomial fits to the data.

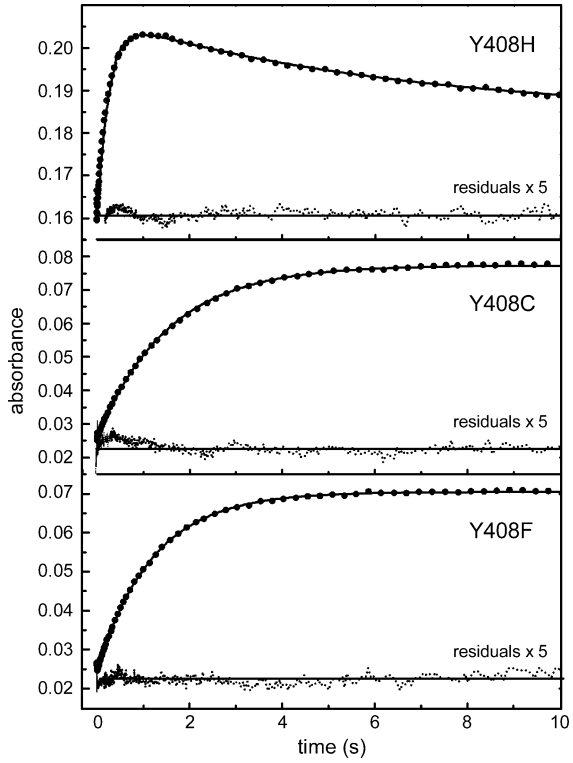

FIGURE 9: Time course of PCA binding to the mutant 3,4-PCD enzymes. All experiments were run anaerobically at 4 °C in 1 M Tris, pH 8.5. Enzyme was mixed with 8 mM PCA to initiate the reaction. 59 μM Y408H enzyme was monitored at 500 nm, 38 μM Y408C enzyme was monitored at 700 nm, and 30 μM Y408F enzyme was monitored at 700 nm. Double (top panel) or single (bottom two panels) summed exponential fits (solid lines) are overlaid on the data (circles, 5% of the data points shown for clarity), with the residuals indicated at the bottom of each plot.

(*31*). Addition of the inhibitor terephthalate (1,4-benzenedicarboxylate) causes this vibration to broaden, suggesting that it has unresolved contributions from both tyrosines in the resting wild-type enzyme (data not shown). Since this feature is also present in spectra of the mutant enzymes, and is relatively unperturbed by the addition of 4HB, it is probably due to the Tyr447$^{O\eta}$−Fe bond. Upon addition of 4HB, higher energy ν Fe−O vibrations are observed (vibrations for each 4HB complex are listed in Table 6). The assignment of these bands to the 4HB^{O4}−Fe bond is consistent with their 10 cm^{-1} decrease in energy upon isotopic labeling of the hydroxyl of 4HB with ^{18}O (Figure 7B). In the Y408C and Y408F mutants, a second, less intense peak in this region also shifts upon isotopic labeling, implying that 4HB may be bound in two conformations. The position of this second peak overlaps with the single peak in the Y408H spectrum. Thus, 4HB may also bind to the Y408H mutant in two conformations that coincidentally produce the same energy ν 4HB^{O4}−Fe vibration. The same mutation-specific pattern noted in the absorption spectra is also observed in this transition. The ν 4HB^{O4}−Fe vibration of the Y408H mutant is nearly the same energy as that in the wild-type enzyme, but these vibrations in the Y408C and Y408F mutants are about 20 cm^{-1} higher in energy. Moreover, although the ν Tyr447$^{O\eta}$−Fe vibration varies little among different mutants, the energy of this transition is about 10 cm^{-1} greater in the mutant enzymes than in the wild type, indicative of a stronger bond between the iron and the axial tyrosine.

Steady-State and Transient Kinetics. At 25 °C in 50 mM Tris and 2 mM β-mercaptoethanol, pH 8.5, under saturating PCA and O_2 conditions, the rate of turnover per Fe(III) for the wild-type enzyme (100 ± 10 s^{-1}) is significantly greater than the turnover numbers of the mutant enzymes Y408C (0.13 ± 0.03 s^{-1}), Y408F (0.011 ± 0.003 s^{-1}), Y408E (0.010 ± 0.003 s^{-1}), and Y408H (0.007 ± 0.002 s^{-1}). In all cases, activity maximized around pH 8.5, and the correct ring-opened product formed in at least 99% yield as determined by optical spectroscopy. Although the turnover numbers of the mutants are too low to allow accurate determination of K_m values, information about ligand affinity during turnover was obtained by determining rates of the individual steps in the ligand binding process of the catalytic cycle as described below.

Stopped-flow spectroscopy was used to monitor the anaerobic binding of substrate. Under pseudo-first-order conditions, the binding of PCA to the Y408C and Y408F mutants was observed to occur in a single-exponential phase (Figure 9). The reciprocal relaxation times (RRTs) were not linearly dependent on substrate concentration for either mutant (see below), suggesting that the actual addition of substrate occurs in a fast, reversible step preceding the one observed. The apparent lack of any change in absorbance from the spectrum of the resting enzyme at the earliest observable time point implies that this unobservable step does not affect the iron ligation, consistent with substrate binding in the hydrophobic active site pocket but not to the iron. The crystal structure of the wild-type enzyme bound with

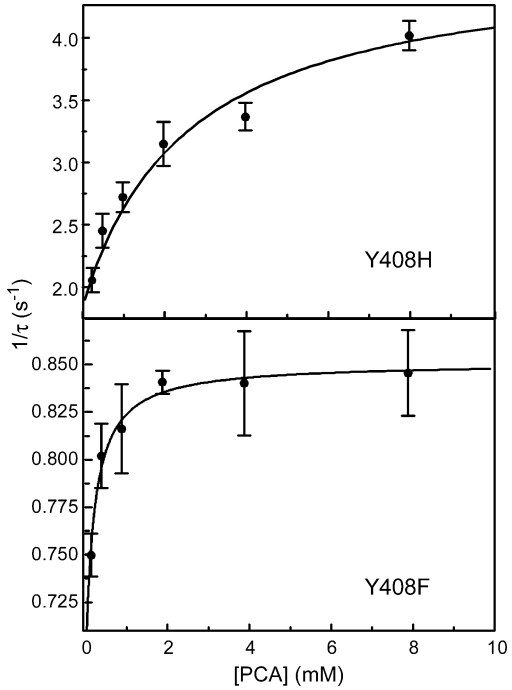

FIGURE 10: Concentration dependence of the RRTs of the PCA binding reactions. Conditions are the same as described in Figure 9, except for variation in the PCA concentration. The average RRTs ($1/\tau$) are plotted for the fast exponential phase from the time course for the Y408H enzyme and the single exponential for the Y408F enzyme, with the standard deviation of the data indicated by error bars. Fits with the values indicated in Table 7 are overlaid on the data.

3HB revealed this type of ligand association, and we have postulated that it is the first step in binding for all aromatic ligands (*7*). In this two-step binding scenario, the absorbance change of the observable step would represent ligation to the iron and formation of the monodentate PCA complexes observed in the crystal structures of the mutated enzymes. This type of two-step reaction gives rise to a hyperbolic dependence of the observed RRT on substrate concentration if the substrate dissociation rate constant is fast relative to the rate constant for coordination to the iron. In the case of the Y408F mutant, a good fit to a hyperbolic function was observed, allowing the calculation of the forward (k_{+2}) and reverse (k_{-2}) rate constants for iron coordination, the K_1 value of the initial substrate complex, and the K_d value for substrate binding to the enzyme overall in the observable steps (see Experimental Procedures) (Figure 10 and Table 7). In the case of the Y408C mutant, the RRT is independent of substrate concentration, implying either that an irreversible step occurs between the substrate association step and the step in which PCA coordinates to the iron or that K_1 is small so that the complex is saturated at low PCA concentrations. In either case, the observed RRT yields approximately the sum of rate constants for the step in which substrate binds to the iron (Table 7).

The binding of PCA to the Y408H enzyme was observed to proceed with a time course reproduced by the sum of one positive and one negative exponential phase (Figure 9), indicating that the reaction involves at least two observable steps. As shown in Figure 10, the RRT of the faster phase has a hyperbolic dependence on substrate concentration while no substrate concentration dependence was observed for the slower (data not shown). Fitting the observed RRT for the first phase to a hyperbola gives approximate values of k_{+2}, k_{-2}, K_1, and K_d (Figure 10 and Table 7). The presence of two phases in the binding of PCA to Y408H may indicate that the binding reactions for the other mutants also involve a low-amplitude second phase. Kinetic evidence in support of this possibility is presented below.

Table 7: Rates (s^{-1}) and Dissociation Constants (μM) Derived from Transient Kinetics at 4 °C[a]

	PCA					4HB				
	k_{+2}	k_{-2}	$k_{+2}+k_{-2}$	K_1	K_d	k_{+2}	k_{-2}	$k_{+2}+k_{-2}$	K_1	K_d
wild type[b]						42	14	56	700	170
Y408H[c]	2.8	1.9	4.7	2600	1100			2.3		
Y408C			0.67					0.7[d]		
Y408F	0.39	0.46	0.85	84	45			0.9[d]		

[a] The experiments were conducted as described in Experimental Procedures. Errors are ±10%. [b] PCA binds to the wild-type enzyme very rapidly to form a complex within the dead time (1.3 ms) of the stopped-flow instrument. [c] A second exponential with a negative amplitude was also observed for PCA binding (Figure 9). [d] A second exponential was observed for the Y408C and Y408F enzymes with a RRT of 0.2 s^{-1} (Figure 12). The amplitude of this second exponential was 85% and 30% of the amplitude of the first exponential for the Y408C and Y408F enzymes, respectively.

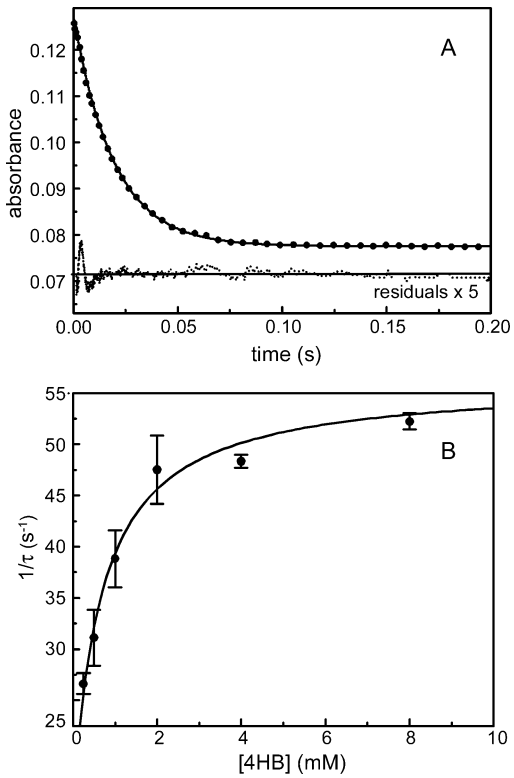

FIGURE 11: Time course and concentration dependence of 4HB binding to wild-type 3,4-PCD. All experiments were run at 4 °C in 1 M Tris, pH 8.5. (A) 53 μM enzyme was mixed with 8 mM 4HB and monitored at 550 nm. (B) The average $1/\tau$ values of the single exponential are plotted for various [PCA] with the standard deviation of the data indicated by error bars. Fits (solid lines) are overlaid on the data (circles, 5% of the data points shown for clarity), with residuals in (A) indicated at the bottom of the plot.

The binding of 4HB to the wild-type and mutant 3,4-PCDs was also monitored under pseudo-first-order conditions. The binding to wild-type 3,4-PCD (Figure 11A) occurred in one observable phase and conformed to the two-step model described above, i.e., a reversible unobserved step with little

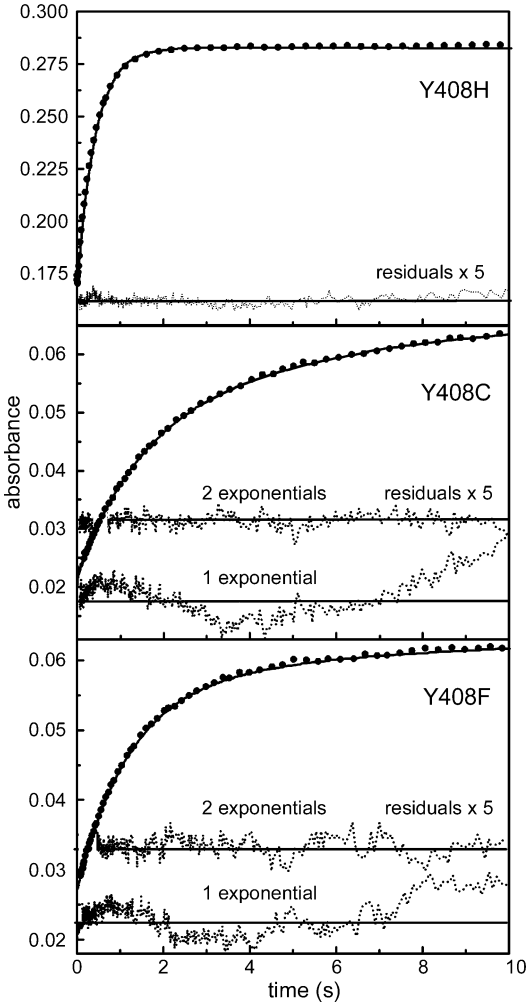

FIGURE 12: Time course of 4HB binding to the mutant 3,4-PCD enzymes. All experiments were run at 4 °C in 1 M Tris, pH 8.5, and mixed with 8 mM 4HB. 35 μM Y408H enzyme was monitored at 470 nm, 38 μM Y408C enzyme was monitored at 700 nm, and 30 μM Y408F enzyme was monitored at 700 nm. Fits (solid line) are overlaid on the data (circles, 5% of the data points shown for clarity), with the residuals indicated at the bottom of each plot. For comparison, the residuals from a single-exponential fit are indicated below the residuals from the double-exponential fit for the Y408C and Y408F enzymes.

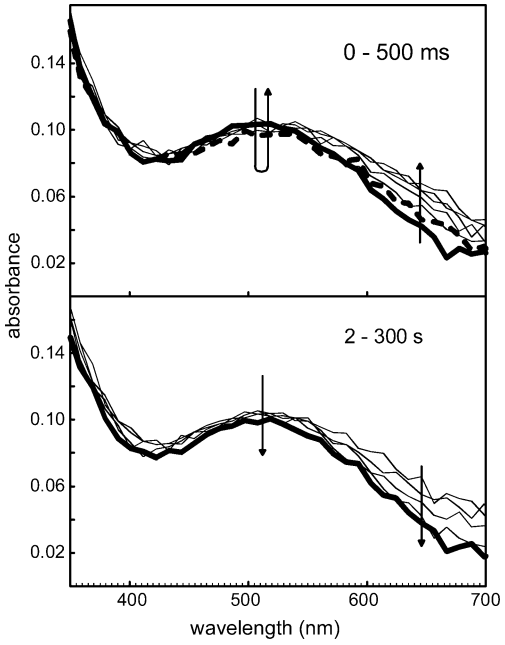

FIGURE 13: The reaction of the Y408C enzyme with PCA and O_2. The experiment was run at 25 °C in 50 mM Tris and 2 mM β-mercaptoethanol, pH 8.5. At 625 μM O_2, 56 μM Y408C was mixed with 28 μM PCA (concentrations after mixing). Top: Diode array spectra acquired at 3.8, 40, 80, 214, 378, 442, and 508 ms are shown. The 4 ms trace is shown as a bold solid line and is similar to the spectrum of the resting enzyme. The second trace at 40 ms is shown as a bold dashed line to emphasize the changes that occur during the first phase of the reaction. Bottom: Diode array spectra from the same reaction at 2.14, 11.66, 25.5, 103, and 291 s. The final trace is shown in bold and again resembles the spectrum of the resting enzyme. The arrows in each panel indicate the direction of OD change.

absorbance change followed by binding to the iron. Accordingly, the 4HB concentration dependence of the single observable phase is hyperbolic (Figure 11B), allowing the k_{+2}, k_{-2}, K_1, and K_d values to be determined (Table 7).

For the Y408H mutant, the 4HB binding reaction also occurs in a single-exponential phase as shown in Figure 12. The time courses of the binding of 4HB to the Y408C and Y408F enzymes were best fit by two summed exponentials (Figure 12), showing that at least two steps are involved. All of the RRTs for these binding reactions to the mutant enzyme are independent of inhibitor concentration, suggesting that there is a fast, effectively irreversible step preceding coordination of 4HB to the iron. The direct optical titrations (Table 5) suggest that this is due to a low value for K_1. All constants for the mutant enzymes are listed in Table 7.

Reaction with Oxygen. Due to the low solubility of O_2, proper pseudo-first-order conditions could not be established. However, the general characteristics of this reaction for the mutant enzymes were determined by mixing Y408C with a slightly substoichiometric concentration of PCA in O_2-saturated buffer to approximate a single turnover under pseudo first-order conditions in O_2. The reaction was monitored at 25 °C to accelerate the slow O_2 reaction and allow a direct comparison with the experimentally determined turnover number (0.13 s^{-1}). The top panel of Figure 13 shows diode array spectra of the first 500 ms of this reaction. A very rapid phase is complete within the first 30 ms that results in a red shift and a slight decrease in absorbance at 500 nm. This is accompanied by a small increase in 650 nm absorbance. Then a slower increase in 650 nm absorbance occurs, leading to formation of a species with the spectrum of the enzyme−substrate complex (see Figure 5). As shown in the bottom panel of Figure 13, the enzyme−substrate complex then very slowly decays smoothly back to a species with the spectrum of the free enzyme, presumably as the oxygen reaction occurs and product is released. Unlike the reaction for the wild-type enzyme (*8*, *32*) and mutants at the Y447 position (*10*), no intermediate spectrum characteristic of the enzyme−PCA−oxygen complex or the enzyme−product complex was detected. A single-wavelength time course is shown in Figure 14. The initial substrate binding process is comparable to that shown in Figure 9 except that it occurs at a much higher rate at 25 °C. A low-amplitude, very fast phase is detected that may be due to the initial, second-order substrate binding process that is visible in this case due to the low PCA concentration. This is followed by the slower ($1/\tau = 5.5$ s^{-1}) binding of PCA to the iron, resulting in the large increase in absorbance. A plateau region is then observed followed by a slow decline

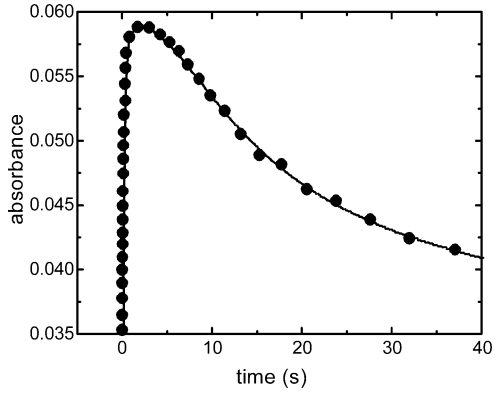

FIGURE 14: Time course of the Y408C mutant reaction with PCA and O_2. The reaction from Figure 13 was monitored at 650 nm with a single-wavelength detector to provide better time resolution (circles, with only every 16th data point shown for clarity). The solid line is the result of a numerical integration of Scheme 2 shown in the text. The rate constants used in the simulation were $k_1 = 1 \times 10^6$ M^{-1} s^{-1}, $k_{-1} = 100$ s^{-1}, $k_2 + k_{-2} = 5.5$ s^{-1}, $k_3 + k_{-3} = 0.22$ s^{-1}, and $k_4 = 0.16$ s^{-1}.

Scheme 2: Proposed Intermediates in the Reaction of Y408C with PCA and O_2

$$E + PCA \underset{k_{-1}}{\overset{k_1}{\rightleftharpoons}} E_1^{PCA} \underset{k_{-2}}{\overset{k_2}{\rightleftharpoons}} E_2^{PCA} \underset{k_{-3}}{\overset{k_3}{\rightleftharpoons}} E_3^{PCA} \xrightarrow[O_2]{k_4} E^{Prod} \xrightarrow[Fast]{Product} E$$

as oxygen reacts with the enzyme−PCA complex to form product. The most likely explanation for the plateau region is that a second, relatively slow, step in the substrate binding process occurs with little absorbance change. A similar step was observed for the PCA binding reaction to Y408H (see Figure 9) and the 4HB binding reactions for Y408C and Y408F (Figure 12), so it is reasonable that this may also occur for the PCA binding reaction with Y408C. This time course is too complex to reliably fit using nonlinear regression techniques, but a fit using a numerical integration simulation of the reaction sequence shown in Scheme 2 (where any of the first-order steps could be reversible) yielded the solid curve shown superimposed on the data.

The rate constant for the initial reaction following the substrate binding steps was estimated from the simulation to be 0.16 s^{-1}, which is about the same as the turnover number. This is assigned to the oxygen reaction step, as opposed to the product release step that is rate limiting for the wild-type enzyme reaction, because it proceeds from the final enzyme−substrate complex and the spectrum of an enzyme−product complex is not observed. Thus, it seems likely that the reaction with O_2 is very slow and rate limiting during turnover.

DISCUSSION

Mutation of the equatorial iron ligand Tyr408 of 3,4-PCD to a variety of other residues is shown here to result in the loss rather than the replacement of an endogenous ligand at the iron due to the inherent rigidity of the metal environment. Remarkably, the presence of new residues near the iron causes significant changes in the spectroscopic and kinetic properties of the enzyme that are not unlike those we might have anticipated for exchange of the metal ligand. The introduction of these new second-sphere residues is observed to result in a large decrease in the rate of the reaction with O_2 caused at least in part by significant decreases in the rate constants of endogenous and exogenous ligand exchange. The latter effect appears to correlate with a change in the Lewis acidity of the iron that alters ligand affinity. These changes offer insights into the multiple roles of the iron ligands in the mechanism of 3,4-PCD and the importance of second-sphere effects in metalloenzyme catalysis, which are discussed in the following sections.

Kinetics of Ligand Binding. The studies presented here show that the binding of 4HB and PCA to the mutant enzymes occurs with rate constants 3−4 orders of magnitude smaller than observed for binding to wild-type 3,4-PCD. In the case of PCA, either the concentration dependence of the binding is hyperbolic (Y408H and Y408F) or none is observed (Y408C). These results are consistent with rapid formation of an initial complex followed by formation of a bond with the metal. Several aspects of these reactions are significant: (i) the time scale of the coordination to the metal is always much longer than that of initial binding to the enzyme active site pocket, suggesting that ligand displacement and/or structural rearrangements are required for the former process; (ii) at least some of the binding reactions to the metal are readily reversible with equilibrium constants near unity, suggesting that the metal−hydroxide (or alternative negatively charged solvent ion) and metal−phenolate bonds are approximately isoenergetic; (iii) the metal binding reactions are much slower in the case of the mutants than for wild-type 3,4-PCD; and (iv) the metal binding reactions for the Y408H mutant are faster than for the Y408C or Y408F mutants. Each of these aspects of the kinetics is consistent with an increase in the Lewis acidity of the iron in the mutant enzymes relative to wild-type 3,4-PCD and is directly related to our proposal for the mechanism of 3,4-PCD as discussed below.

Our model for the mechanism of 3,4-PCD (Scheme 1), supported by crystallographic studies of substrate and inhibitor complexes (*6*, *7*, *33*), is based on the concept that each step in substrate binding, oxygen reaction, and product release is facilitated by a specific change in the metal ligation. Accordingly, it is reasonable that the protein scaffold around the active site metal is rigidly constructed so that the structural changes necessary for catalysis proceed in a defined fashion. This has now been amply demonstrated by our mutation studies of metal ligands in both the axial and equatorial positions. When ligands are replaced with residues of greater length, the strain imposed by the backbone causes steric overlap and destabilization of the bound iron.[4] When ligands are replaced with residues of shorter length, the backbone is unperturbed and a gap is created between the residue and the iron. Our studies have shown that this gap is filled by a solvent molecule to maintain the coordination geometry. For example, in the resting state of the Y447H mutant, the open axial metal ligand site generated by mutation is occupied by one oxygen of a bidentate carbonate molecule (*10*). In this report, it is shown that a molecule of water replaces Tyr408 in the iron coordination of each of the mutant enzymes. The presence of this solvent molecule

[4] Replacement of either histidine ligand in 3,4-PCD with a tyrosine results in enzymes that cannot bind iron. This has been observed both in our site-directed studies with the *P. putida* enzyme (Valley et al., unpublished results) and in a random mutant (H460Y) generated in the *Acinetobacter calcoaceticus* enzyme (*34*).

opens the possibility of second-sphere effects on catalysis by the new 408 residue transmitted through interaction with the solvent.

The new water ligand of these Tyr408 mutants is a weaker Lewis base than tyrosinate, and thus the Lewis acidity of the iron should increase in all cases and be reflected in stronger metal−ligand interactions. This is consistent with our findings that the inhibitor 4HB binds to the iron in the mutant enzymes to form a monodentate complex with a lower K_d and a higher energy Fe−O vibration than that observed in the wild-type inhibitor complex (Tables 5 and 6). The rates at which substrates and inhibitors bind to the iron also support this conclusion. The rates at which ligands initially bind in the active site pocket would not be expected to be altered by mutation of the iron ligands, and these rates are observed to remain fast. However, the crystal structures of the mutant enzyme−PCA complexes show that the subsequent binding to the iron requires displacement of the bound solvent (hydroxide, or alternative small anion). This seems to be an inherent part of the general ligand binding mechanism to the iron of 3,4-PCD, which involves the exchange of anionic species. In effect, the anionic solvent ligand bound to the iron must dissociate and act as an in situ base to deprotonate the hydroxyl function of PCA or 4HB to allow it to bind to the iron. The slow binding of PCA and 4HB to the iron in the mutant enzymes may reflect slow dissociation of the solvent due to the higher affinity of the more Lewis acidic iron for anionic ligands. However, once the exchange has occurred, the anionic phenolate or catecholate ligands will also be bound tightly, perhaps comparably with the anionic solvent as indicated by the kinetics of the binding process.

Slow ligand exchange can be considered a manifestation of the principle of charge maintenance that appears to pertain to 3,4-PCD and many other metalloproteins (*7*, *10*, *35*−*43*). The active sites of these enzymes are balanced such that, as the catalytic cycle progresses, changes in ligand type or ionization state maintain the original net charge of the active site. Deviation from this charge is thought to provide a driving force to restore the original charge and, in doing so, carry the enzyme to the next intermediate in the reaction cycle. When Tyr408 is removed from the Fe(III) coordination sphere of 3,4-PCD, the iron environment takes on a positive net charge. Accordingly, the metal should display a high affinity for negative ligands to move the net charge back toward that for which the active site structure was designed.

Perhaps the most mechanistically significant ramification of the increased Lewis acidity of the iron is the failure of Tyr447 to dissociate during PCA binding. In the wild-type enzyme, dissociation of Tyr447 both promotes deprotonation of the second OH group of PCA and provides a place for it to bind to the Fe(III). A dianionic catecholate complex appears to be required for rapid turnover because the O_2 is thought to attack the substrate by an electrophilic mechanism. In general, the chelate would be expected to be more stable than the monodentate complex, but because the chelate complex does not form even over the time required to collect crystallographic data, there appears to be a substantial kinetic barrier to its formation in the mutants. The origin of this barrier is postulated to be the high affinity of the overly Lewis acidic iron for Tyr447 preventing its dissociation. This is consistent with the increase in strength of the $Tyr447^{O\eta}$−Fe bond in the mutants revealed by its 10 cm^{-1} increase in vibrational energy. Thus, in the resting mutant enzymes, ligands such as Tyr447, and to some extent the anionic solvent, become substitution inert, slowing or blocking the natural catalytic cycle.

Although there is strong spectroscopic evidence for strengthening of the iron phenolate and catecholate bonds in the mutant enzyme in solution, the crystal structures do not show the expected shorter Fe−O bonds. It is possible that the resolution of the current structures (∼2.1 Å) does not allow the expected 0.1 Å differences to be resolved. Alternatively, the position of the iron is different in the mutant enzymes so that direct distance comparisons may not be valid. Removal of the Y408 ligand reduces steric constraints that distorted the iron coordination geometry such that the iron−ligand bonds relax to a more ideal geometry, which may contribute to the observed increase in bond strength since the backbone position does not also shift.

Second-Sphere Effects. Although each of the Tyr408 mutants increases the affinity of the active site iron for anionic ligands, there are significant differences between the spectroscopic and kinetic properties of the individual mutants. This is particularly apparent in the effects that the different 408-position residues have on ligands bound in the active site on the opposite side of the iron. The mutants fall roughly into two groups. The Y408C and Y408F enzymes form higher energy Fe−O bonds with ligands, exhibit lower energy LMCT bands, and support a slower rate of ligand exchange compared to the Y408H and Y408E enzymes. On the basis of the crystal structures, it seems likely that this is due in part to the ability of the altered residue in the latter two mutants to hydrogen bond directly to the new water molecule in the iron coordination sphere, thereby increasing its anionic character and increasing its trans effect on substrates and inhibitors. In contrast, the thiolate of Cys408 and the aromatic ring of Phe408 in their respective mutants either are too short (Cys) or contain no appropriate functionality (Phe), and thus they cannot form a direct hydrogen bond with the new solvent ligand.

The degree of anionic character of the solvent in the position normally occupied by Tyr408 is manifested as a blue shift in the λ_{max} of the spectra of the PCA and 4HB complexes of the mutant enzymes (Figure 5). The trans effect of the additional charge on the solvent proposed to be caused by hydrogen bonding to the new residues in Y408H and Y408E increases the energy of the LMCT band from the opposite ligand and weakens the iron−exogenous ligand bond. This is evident from a comparison of the resonance Raman spectra of these mutants in which the ν $Fe-O^{4HB}$ vibrations of the Y408C and Y408F enzymes are about 20 cm^{-1} higher in energy than that of Y408H (Table 6). Moreover, the rate constants for ligand binding to the iron in the Y408C and Y408F enzymes are significantly lower, suggestive of slower solvent dissociation due to stronger iron−solvent interactions (Table 7). On the basis of these observations, it is also likely that the anionic Tyr408 ligand of the wild-type enzyme exerts significant effects on the substrate throughout the catalytic cycle, specifically weakening the Fe−O bond in the trans position at each stage and thereby promoting efficient transit from one species to the next.

Multistep Substrate and Inhibitor Binding. The kinetics of binding of PCA to the Y408H mutant and 4HB to the Y408C and Y408F mutants clearly show evidence for a slow step following the initial steps of binding to the enzyme and then to the iron. Past crystallographic studies using inhibitors to mimic the steps in substrate binding suggest that there is a step after formation of a complex between the iron and a catecholic oxygen of the substrate or inhibitor in which the coordination geometry converts from trigonal bipyramidal to octahedral (*7*). This occurs by a movement of the substrate or inhibitor deeper into the active site so that the binding oxygen is more precisely aligned trans to the Tyr408 ligand. Using the Y447H mutant, which slows substrate binding but still yields the correct chelated PCA complex, two steps were observed to occur after the initial binding of substrate to the iron (*10*). It is reasonable that the same type of additional step or steps occurs in the Y408X mutant proteins studied here. Only in some cases does this give rise to an observable change in the chromophore. For the binding of PCA to the Y408C mutant, there is no obvious change in the chromophore, but the additional step in substrate binding can be detected in the reaction with O_2 because a plateau is observed in the kinetic time course which would not be present if O_2 were to react directly with the intermediate formed during the relatively fast association of the PCA^{O4} with the iron. This putative second intermediate in the substrate and inhibitor binding process has ramifications for the K_d values determined by equilibrium titration and dynamic methods. If the additional step has a small reverse rate constant, a significantly lower K_d will be observed for the equilibrium titration methods. This appears to pertain to at least some of the binding reactions. For example, PCA binding by Y408H exhibits a K_d value which is almost 2 orders of magnitude lower when determined by equilibrium titration than from the transient kinetic data.

Kinetics of the Reaction of Y408C with Oxygen. Past studies of the reaction of O_2 with the 3,4-PCD−substrate complex have revealed rapid second-order kinetics with a rate constant in excess of 10^5 M^{-1} s^{-1} (*8*, *32*). The intermediate formed in this process exhibits a bleached optical spectrum and converts rapidly to an enzyme−product complex characterized by a more intense optical spectrum that has a characteristic plateau through the 450−550 nm visible region. The same species is observed for the long-lived product complex in the Y447H mutant of 3,4-PCD (*10*). It is significant that neither of these spectroscopically distinct species is observed during the time course of the reaction of Y408C with PCA and O_2, despite the fact that the reaction occurs on a time scale that should make the observation of any intermediates straightforward. Because the rate constant for the reaction that results in the initial loss of the spectroscopic features for the enzyme−substrate complex is similar to the overall turnover number, it is likely that the O_2 reaction itself is rate limiting in catalysis. On the basis of the mechanism we have proposed for the O_2 reaction (Scheme 1), the slow rate for Y408C and the other mutants is not unexpected. We propose that the ability of O_2 to attack the substrate depends on the anionic character of the substrate, which is relatively low in the case of the mutant enzymes where the substrate is bound as a monoanion. Indeed, it appears that there is no alternative way to stabilize the dianion in the active site because 4-NC, which forms a dianionic species more readily than PCA, is also bound as the monoanion in the active site.

Mechanism of the Mutant Enzymes. The observed turnover numbers of the Tyr408 mutants are 1000-fold or more below that of the wild-type enzyme and differ from one another over a 10-fold range. The rate-limiting step for the wild-type enzyme is the release of product, with both the substrate binding and O_2 reaction steps occurring much more rapidly (*8*, *32*). In contrast, the current results suggest that the Tyr408 mutants are rate limited by O_2 reactivity. Even at 4 °C, the substrate binding steps have rate constants that exceed the turnover number at 25 °C, and the slow reaction of the enzyme−substrate complex with O_2 is easily monitored at 25 °C. We propose that the reaction with O_2 is slow because the substitution inert iron of the mutant enzymes prevents dissociation of Tyr447. Thus, the base required to deprotonate the second OH of the substrate is absent, and the substrate is trapped as the monoanion which is much less reactive with electrophilic O_2.

Why do the mutant enzymes differ from one another in turnover number? One possibility, suggested by the observation of the normal ring cleavage product, is that a small fraction of the time the Tyr447 ligand does dissociate in each of the mutants, thereby allowing the substrate to assume the chelated orientation and the charge on the trans solvent to affect the rate of O_2 reactivity. One argument against this is that this would place the new solvent molecule opposite PCA^{O3}. The putative increased anionic character of this solvent in the Y408H and Y408E mutants would be more similar in effect to the native Tyr408 and would presumably support a higher rate of turnover, but this is not the case. The highest rate of turnover is obtained with the Y408C mutant, which, it seems, has the solvent with the lowest anionic character.

It is also possible that the PCA reacts without rotating to the chelated position if a small amount of the dianion forms by ionization of the C3-OH group to promote substrate ketonization and carbanion formation at C4. This would be promoted by charge delocalization onto the iron from the PCA^{O4} through strong bond formation just as it is in the wild-type enzyme. In the latter case, the strong PCA^{O4} bond is promoted by binding trans to a neutral His462 ligand. For the Y408C mutant, the PCA^{O4} appears to bind trans to a neutral water in contrast to the more charged solvent present for the other mutants. Thus, formation of a PCA carbanion would be more favorable for the Y408C mutant, resulting in a higher turnover rate.

It is, perhaps, useful to consider the differing effects of mutations at the Tyr447 and Tyr408 positions as illustrated in Scheme 3. At the outset of our investigations of the roles of these two ligands, we predicted that mutants at the 447 position would affect substrate binding and product release steps of the catalytic cycle because this residue serves to deprotonate the incoming substrate and protonate the exiting product. This was borne out in studies of the Y447H mutant (*10*) in which the multiple steps in substrate binding and product release occur slowly, allowing them to be resolved. Because Tyr447 dissociates during PCA binding, the Y447H mutant might be expected to show nearly normal O_2 reaction kinetics, and this was also found to be the case. In contrast, the major role for Tyr408 was predicted to be in the O_2 reaction phase of the cycle, specifically acting to establish

Scheme 3: Proposal for the Basis of the Different Effects of the Y447H and Y408C Mutations on O_2 Reactivity[a]

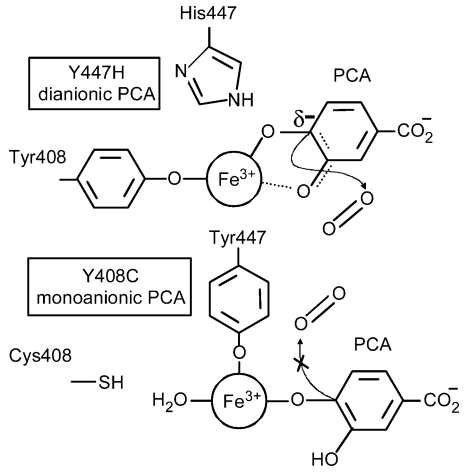

[a] Two aspects of the Y447H structure increase the O_2 reactivity despite the same ligand set as Y408C. First, Y447H has an open axial ligand site to allow PCA to chelate as a dianion. Second, Tyr408 is in position to create an asymmetric PCA chelate through trans effects.

the asymmetric substrate binding that directs the position and, to some extent, the rate of O_2 attack. Indeed, this still may be an important role for this residue in the wild-type enzyme. However, the great decrease in O_2 reaction rate demonstrated in this study is not caused by this effect because the substrate does not rotate into the chelated position. The current study reveals a potentially even more significant role for Tyr408 in establishing a metal center poised to allow ligand exchange. It is interesting that both the Y447H and Y408H mutations yield iron centers with the same ligand set, and each causes a comparable decrease in overall rate, but the origin of the decrease is completely different.[5] This clearly illustrates the importance of both the type and position of the metal ligands for catalysis.

Comparison of Catalysis in Model Systems versus 3,4-PCD. Model complexes have also been used to study the intradiol enzyme reaction. These studies appear to support a different correlation between the Lewis acidity of the iron and activity than we report here. In one specific study, a series of tetradentate ligands were synthesized with a central tertiary nitrogen linked to a varying combination of carboxylates and pyridines (*44*, *45*). These ligands formed a complex with iron and a di-*tert*-butylcatechol substrate, which upon exposure to oxygen yielded intradiol cleavage products. It was observed that as the Lewis base strength of the tetradentate ligand was decreased by replacing carboxylates with pyridines, the rate and yield of product formation increased. This suggests that increasing the Lewis acidity of the iron in 3,4-PCD by decreasing the Lewis base strength of the ligands through mutagenesis should enhance catalysis. In contrast, it is shown here that increasing the Lewis acidity of the iron by mutating Tyr408 dramatically decreases the rate of the reaction. It is important to recognize that the decrease in reaction rate for the enzyme occurs because the change in ligands makes the iron center substitution inert so that the reactive chelated dianionic form of the substrate is not presented to oxygen. Thus, the effect of a change in Lewis acidity specifically on the reaction of O_2 with the catecholic substrate is not being uniquely examined. Indeed, within the series of mutants, the most Lewis acidic iron (Y408C) is the best catalyst, and this may better reflect the true differences in substrate activation for electrophilic attack (see above). These results show that, in contrast to the model systems, the primary factor for efficient catalysis by the enzyme is not the actual reaction rate with O_2 but rather the rate of the complete process from substrate binding to product release. Our studies show that the choice and placement of iron ligands are critical to these aspects of catalysis. Thus, the metal center in 3,4-PCD appears to be poised optimally for efficient catalysis; the Lewis acidity of the iron is high enough to promote the charge localization on PCA necessary for electrophilic attack, yet low enough to allow the necessary ligand rearrangements for rapid turnover.

[5] Indeed, it is likely that the Lewis acidity of the iron in these two mutants is similar and also induces decreased exchange rates in Y447H as observed for Y408H. In the former case, however, the axial ligand site required to form the PCA chelate complex is vacant, allowing this critical complex to form and oxygen to rapidly react to form the product complex. This final complex releases product very slowly.

ACKNOWLEDGMENT

The authors thank Drs. Raymond Y. N. Ho and Lawrence Que, Jr., for assistance in collection and interpretation of resonance Raman spectra.

REFERENCES

1. Lipscomb, J. D., and Orville, A. M. (1992) Mechanistic aspects of dihydroxybenzoate dioxygenases, *Metal Ions Biol. Syst. 28*, 243−298.
2. Que, L., and Ho, R. Y. N. (1996) Dioxygen activation by enzymes with mononuclear non-heme iron active sites, *Chem. Rev. 96*, 2607−2624.
3. Stanier, R. Y., and Ornston, L. N. (1973) The beta-ketoadipate pathway, *Adv. Microb. Phys. 9*, 89−151.
4. Ohlendorf, D. H., Lipscomb, J. D., and Weber, P. C. (1988) Structure and assembly of protocatechuate 3,4-dioxygenase, *Nature 336*, 403−405.
5. Ohlendorf, D. H., Orville, A. M., and Lipscomb, J. D. (1994) Structure of protocatechuate 3,4-dioxygenase from *Pseudomonas aeruginosa* at 2.15 Å resolution, *J. Mol. Biol. 244*, 586−608.
6. Orville, A. M., Lipscomb, J. D., and Ohlendorf, D. H. (1997) Crystal structures of substrate and substrate analog complexes of protocatechuate 3,4-dioxygenase: Endogenous Fe^{3+} ligand displacement in response to substrate binding, *Biochemistry 36*, 10052−10066.
7. Orville, A. M., Elango, N., Lipscomb, J. D., and Ohlendorf, D. H. (1997) Structures of competitive inhibitor complexes of protocatechuate 3,4-dioxygenase: Multiple exogenous ligand binding orientations within the active site, *Biochemistry 36*, 10039−10051.
8. Bull, C., Ballou, D. P., and Otsuka, S. (1981) The reaction of oxygen with protocatechuate 3,4-dioxygenase from *Pseudomonas putida*. Characterization of a new oxygenated intermediate, *J. Biol. Chem. 256*, 12681−12686.
9. Whittaker, J. W., and Lipscomb, J. D. (1984) Transition state analogs for protocatechuate 3,4-dioxygenase. Spectroscopic and kinetic studies of the binding reactions of ketonized substrate analogs, *J. Biol. Chem. 259*, 4476−4486.
10. Frazee, R. W., Orville, A. M., Dolbeare, K. B., Yu, H., Ohlendorf, D. H., and Lipscomb, J. D. (1998) The axial tyrosinate Fe^{3+} ligand in protocatechuate 3,4-dioxygenase influences substrate binding and product release: Evidence for new reaction cycle intermediates, *Biochemistry 37*, 2131−2144.
11. Fox, B. G., Froland, W. A., Dege, J. E., and Lipscomb, J. D. (1989) Methane monooxygenase from *Methylosinus trichosporium* OB3b. Purification and properties of a three-component system with high specific activity from a type II methanotroph, *J. Biol. Chem. 264*, 10023−10033.
12. Frazee, R. W., Livingston, D. M., LaPorte, D. C., and Lipscomb, J. D. (1993) Cloning, sequencing, and expression of the *Pseudo-*

monas putida protocatechuate 3,4-dioxygenase genes, *J. Bacteriol. 175*, 6194−6202.
13. Strickland, S., Palmer, G., and Massey, V. (1975) Determination of dissociation constants and specific rate constants of enzyme−substrate (or protein−ligand) interactions from rapid reaction kinetic data, *J. Biol. Chem. 250*, 4048−4052.
14. Howard, A. J., Gilliland, G. L., Finzel, B. C., Poulos, T. L., Ohlendorf, D. H., and Salemme, F. R. (1987) Use of an imaging proportional counter in macromolecular crystallography, *J. Appl. Crystallogr. 20*, 383−387.
15. Pflugrath, J. W. (1999) The finer things in X-ray diffraction data collection, *Acta Crystallogr., Sect. D 55*, 1718−1725.
16. Jones, T. A., Zou, J. Y., Cowan, S. W., and Kjeldgaard, M. (1991) Improved methods for finding protein models in electron density maps and the location of error in these models, *Acta Crystallogr., Sect. A 47*, 110−119.
17. Brünger, A. T., Adams, P. D., Clore, G. M., DeLano, W. L., Gros, P., Grosse-Kunstleve, R. W., Jiang, J. S., Kuszewski, J., Nilges, M., Pannu, N. S., Read, R. J., Rice, L. M., Simonson, T., and Warren, G. L. (1998) Crystallography & NMR system: A new software suite for macromolecular structure determination, *Acta Crystallogr., Sect. D 54*, 905−921.
18. Hooft, R. W. W., Vreind, G., Sander, C., and Abola, E. E. (1996) Errors in protein structures, *Nature 381*, 272.
19. Laskowski, R. A., MacArthur, M. W., Moss, D. S., and Thornton, J. M. (1993) Procheck: A program to check the stereochemical quality of protein structures, *J. Appl. Crystallogr. 26*, 283−291.
20. Christopher, J. A. (1998) SPOCK: The structural properties observation and calculation kit, Texas A&M University, College Station, TX.
21. Orville, A. M., Harpel, M. R., and Lipscomb, J. D. (1990) Synthesis of oxygen-17- or oxygen-18-enriched dihydroxy aromatic compounds, *Methods Enzymol. 188*, 107−115.
22. Tyson, C. A. (1975) 4-Nitrocatechol as a colorimetric probe for non-heme iron dioxygenases, *J. Biol. Chem. 250*, 1765−1770.
23. Groce, S. L., Miller-Rodeberg, M. A., and Lipscomb, J. D. (2004) Single-turnover kinetics of homoprotocatechuate 2,3-dioxygenase, *Biochemistry 43*, 15141−15153.
24. Que, L., Jr., Lipscomb, J. D., Zimmermann, R., Münck, E., Orme-Johnson, N. R., and Orme-Johnson, W. H. (1976) Mössbauer and EPR spectroscopy of protocatechuate 3,4-dioxygenase from *Pseudomonas aeruginosa*, *Biochim. Biophys. Acta 452*, 320−334.
25. Siu, C.-T., Orville, A. M., Lipscomb, J. D., Ohlendorf, D. H., and Que, L., Jr. (1992) Resonance Raman studies of the protocatechuate 3,4-dioxygenase from *Brevibacterium fuscum*, *Biochemistry 31*, 10443−10448.
26. Davis, M. I., Orville, A. M., Neese, F., Zaleski, J. M., Lipscomb, J. D., and Solomon, E. I. (2002) Spectroscopic and electronic structure studies of protocatechuate 3,4-dioxygenase: Nature of tyrosinate-Fe(III) bonds and their contribution to reactivity, *J. Am. Chem. Soc. 124*, 602−614.
27. Tatsuno, Y., Saeki, Y., Iwaki, M., Yagi, T., Nozaki, M., Kitagawa, T., and Otsuka, S. (1978) Resonance Raman spectra of protocatechuate 3,4-dioxygenase. Evidence for coordination of tyrosine residue to ferric iron, *J. Am. Chem. Soc. 100*, 4614−4615.
28. Keyes, W. E., Loehr, T. M., and Taylor, M. L. (1978) Raman spectral evidence for tyrosine coordination of iron in protocatechuate 3,4-dioxygenase, *Biochem. Biophys. Res. Commun. 83*, 941−945.
29. Que, L., Jr., and Heistand, R. H., II (1979) Resonance Raman studies on pyrocatechase, *J. Am. Chem. Soc. 101*, 2219−2221.
30. Cox, D. D., Benkovic, S. J., Bloom, L. M., Bradley, F. C., Nelson, M. J., Que, L., Jr., and Wallick, D. E. (1988) Catecholate LMCT bands as probes for the active sites of nonheme iron oxygenases, *J. Am. Chem. Soc. 110*, 2026−2032.
31. Oehrstroem, L., and Michaud-Soret, I. (1996) Quantum chemical approach to the assignment of iron-catecholate vibrations and isotopic substitution shifts, *J. Am. Chem. Soc. 118*, 3283−3284.
32. Fujisawa, H., Hiromi, K., Uyeda, M., Okuno, S., and Nozaki, M. (1972) Protocatechuate 3,4-dioxygenase. 3. An oxygenated form of enzyme as reaction intermediate, *J. Biol. Chem. 247*, 4422−4428.
33. Elgren, T. E., Orville, A. M., Kelly, K. A., Lipscomb, J. D., Ohlendorf, D. H., and Que, L., Jr. (1997) Crystal structure and resonance Raman studies of protocatechuate 3,4-dioxygenase complexed with 3,4-dihydroxyphenylacetate, *Biochemistry 36*, 11504−11513.
34. Gerischer, U., and Ornston, L. N. (1995) Spontaneous mutations in pcaH and -G, structural genes for protocatechuate 3,4-dioxygenase in *Acinetobacter calcoaceticus*, *J. Bacteriol. 177*, 1336−1347.
35. Orville, A. M., and Lipscomb, J. D. (1997) Cyanide and nitric oxide binding to reduced protocatechuate 3,4-dioxygenase: Insight into the basis for order-dependent ligand binding by intradiol catecholic dioxygenases, *Biochemistry 36*, 14044−14055.
36. Han, S., Eltis, L. D., Timmis, K. N., Muchmore, S. W., and Bolin, J. T. (1995) Crystal structure of the biphenyl-cleaving extradiol dioxygenase from a PCB-degrading pseudomonad, *Science 270*, 976−980.
37. Sugimoto, K., Senda, T., Aoshima, H., Masai, E., Fukuda, M., and Mitsui, Y. (1999) Crystal structure of an aromatic ring opening dioxygenase LigAB, a protocatechuate 4,5-dioxygenase, under aerobic conditions, *Structure (London) 7*, 953−965.
38. Senda, T., Sugiyama, K., Narita, H., Yamamoto, T., Kimbara, K., Fukuda, M., Sato, M., Yano, K., and Mitsui, Y. (1996) Three-dimensional structures of free form and two substrate complexes of an extradiol ring-cleavage type dioxygenase, the BphC enzyme from *Pseudomonas* sp. strain KKS102, *J. Mol. Biol. 255*, 735−752.
39. Rosenzweig, A. C., Nordlund, P., Takahara, P. M., Frederick, C. A., and Lippard, S. J. (1995) Geometry of the soluble methane monooxygenase catalytic diiron center in two oxidation states, *Chem. Biol. 2*, 409−418.
40. Elango, N., Radhakrishnan, R., Froland, W. A., Wallar, B. J., Earhart, C. A., Lipscomb, J. D., and Ohlendorf, D. H. (1997) Crystal structure of the hydroxylase component of methane monooxygenase from *Methylosinus trichosporium* OB3b, *Protein Sci. 6*, 556−568.
41. Lee, S. K., and Lipscomb, J. D. (1999) Oxygen activation catalyzed by methane monooxygenase hydroxylase component: Proton delivery during the O−O bond cleavage steps, *Biochemistry 38*, 4423−4432.
42. Holm, R. H., Kennepohl, P., and Solomon, E. I. (1996) Structural and functional aspects of metal sites in biology, *Chem. Rev. 96*, 2239−2314.
43. Groce, S. L., and Lipscomb, J. D. (2005) Aromatic ring cleavage by homoprotocatechuate 2,3-dioxygenase: Role of His200 in the kinetics of interconversion of reaction cycle intermediates, *Biochemistry 44*, 7175−7188.
44. Cox, D. D., and Que, L., Jr. (1988) Functional models for catechol 1,2-dioxygenase. The role of the iron (III) center, *J. Am. Chem. Soc. 110*, 8085−8092.
45. Jang, H. G., Cox, D. D., and Que, L., Jr. (1991) A highly reactive functional model for the catechol dioxygenases. Structure and properties of [Fe(TPA)DBC]BPh_4, *J. Am. Chem. Soc. 113*, 9200−9204.

BI050902I